COMPUTATIONAL STUDIES OF COORDINATIVELY UNSATURATED TRANSITION METAL COMPLEXES

Sridhar Vaddadi, M. Sc. (Tech)

Dissertation Prepared for the Degree of

DOCTOR OF PHILOSOPHY

UNIVERSITY OF NORTH TEXAS

December 2006

APPROVED:

Thomas R. Cundari, Major Professor
Mohammad Omary, Committee Member
Angela K. Wilson, Committee Member
Ruthanne D. Thomas, Chair of the Department of Chemistry
Sandra L. Terrell, Dean of the Robert B. Toulouse School of Graduate Studies

Vaddadi, Sridhar. *Computational Studies of Coordinatively Unsaturated Transition Metal Complexes.* Doctor of Philosophy (Inorganic Chemistry), December 2006, 83 pp., 13 tables, 15 figures, 3 schema, references, 91 titles.

In this research the validity of various computational techniques has been determined and applied the appropriate techniques to investigate and propose a good catalytic system for C-H bond activation and functionalization. Methane being least reactive and major component of natural gas, its activation and conversion to functionalized products is of great scientific and economic interest in pure and applied chemistry. Thus C-H activation followed by C-C/C-X functionalization became crux of the synthesis.

DFT (density functional theory) methods are well suited to determine the thermodynamic as well as kinetic factors of a reaction. The obtained results are helpful to industrial catalysis and experimental chemistry with additional information: since C-X (X = halogens) bond cleavage is important in many metal catalyzed organic syntheses, the results obtained in this research helps in determining the selectivity (kinetic or thermodynamic) advantage. When C-P bond activation is considered, results from chapter 3 indicated that C-X activation barrier is lower than C-H activation barrier.

The results obtained from DFT calculations not only gave a good support to the experimental results and verified the experimentally demonstrated Ni-atom transfer mechanism from Ni=E (E = CH_2, NH, PH) activating complex to ethylene to form three-membered ring products but also validated the application of late transition metal complexes in respective process.

Results obtained supported the argument that increase in metal coordination and electronic spin state increases catalytic activity of Fe^{III}-imido complexes. These results not only encouraged the fact that DFT and multi-layer ONIOM methods are good to determine geometry and thermodynamics of meta-stable chemical complexes, but also gave a great support to spectroscopic calculations like NMR and Mossbauer calculations.

ACKNOWLEDGEMENTS

I wish to acknowledge the role of many people that have been involved in earning of this doctoral degree. I would like to place on record my intimate gratitude to my Ph.D. advisor Dr. Thomas R. Cundari, whom I respect and admire to the core of my belief. His passion and enthusiasm for science and clarity over the minute details in research is commendable. His presence in the lab and benevolent behavior influenced me and inspired me. I would like to thank Dr. Cundari for everything during my course of stay in Department of Chemistry, University of North Texas. I am taking an opportunity to thank my committee for their time and invaluable suggestions to this dessertation. A special note of acknowledgements to Dr. Omary and Dr. Wilson for their constant support and suggestions. I feel so happy and important to owe all my present and past lab mates for their cordial behavior. I would like to express my deep sense of gratitude to our collaborator Dr. Patrick L. Holland from the University of Rochester. The National Science Foundation, Department of Education, Department of Energy, UNT's Faculty Research Grant, Center for Advanced Scientific Computing and Modeling, have provided support for my dissertation work. A note of thanks to all these scientific and financial agencies for their support.

Finally the most important 'part' is to acknowledge my family and friends around the globe for their consistent support. A special note of gratitude is due to my parents and my wife for their encouragement, love and support.

TABLE OF CONTENTS

Page

LIST OF TABLES

Page

LIST OF FIGURES AND SCHEMES

Page

Figures

Schemes

CHAPTER 1

INTRODUCTION

Transition metal complexes are ubiquitous in catalysis and organometallic chemistry. Transition metal complexes with coordinative unsaturation and/or electronic unsaturation are more prone towards catalytic activity. The presence of coordination unsaturation at the metal is often required to facilitate important reactions like carbon-hydrogen activation,[1] ligand substitution reactions,[2] group transfer reactions,[3] and various organic transformations and functionalization.[4] The preceding reactions typically operate through mechanisms involving oxidative addition,[5] reductive elimination,[6] and radical abstraction.[7] The development of computational methods and techniques has elevated the understanding of these reaction mechanisms. Since most of the experimental methods require expensive instrumentation and catalysis involves highly reactive (i.e., short lifetime and very low concentration) chemical intermediates, computational chemistry can play a definitive role as an adjunct to experiment in the analysis and design of catalytic processes. The increasing sophistication of software and methodology, along with greater computer power, now make theory a true compliment to existing experimental methods.

1.1 Overview of Dissertation

This section gives an overview of this dissertation research.

1.1.1 Bond Activation using Iridium(I) Complexes[8]

Carbon-hydrogen and carbon-X (X = heterogroup) bond activation and functionalization comprise one of the most important family of reactions in transition

metal catalysis.[9] Iridium with its multiple formal oxidation states ranging from -1 through +6 plays a prominent role in C-H/X bond activation through oxidative addition mechanisms.[9] In this research B3LYP density functional along with Stevens effective core potentials (ECP) are used to perform a comparative study of C-H/X bond activation. The model complex $Ir(PH_3)_2H$ with CH_3X (X = F, Cl, OH, SH, NH_2, PH_2) substrates has been used to investigate the kinetic and thermodynamic effect of oxidative addition and reductive elimination of C-H/X bond. Analysis of the geometric minima of the reactants and products indicated a significant thermodynamic preference for C-X over C-H activation. However, comparison of transition states for oxidative addition suggested a noteworthy kinetic preference for C-H activation over C-X activation.

1.1.2 Group Transfer from Nickel Complexes

Group transfer reactions, where a multipily-bonded heterogroup is transferred from a terminally bonded transition metal-heterogroup complex to a C=C or C-H bond comprises one of the important reactions in transition metal chemistry. Although the presence of filled $d\pi$ orbitals often negate the formation of stable multiply bonded complexes of late transition metals,[10] recent synthesis of multiply bonded nickel complexes with phosphinidene (PR),[11] carbene (CR_2),[12] and nitrene (NR)[13] ligands by Hillhouse and his group remain among the few examples of stable multiply bonded complexes of the late transition metals. In this research the B3LYP density functional and Stevens effective core potentials are used to study models[14] of the Hillhouse complexes to investigate the kinetic (transition state) and thermodynamic (ground

state) feasibility of Ni=E (E = CH_2, NH, PH) mediated group transfer (E) to ethylene resulting in three-membered ring organic products, cyclo-EC_2H_4. Enthalpy calculations indicate that (dhpe)Ni=E is an effective system for heterogroup transfer. Comparison of activation barriers for the total reaction mechanism lead to the conclusion that reductive elimination is the rate-determining step of the mechanism for all E groups studied.[77]

1.1.3 Role of Spin State and Coordination Number on C-H Activation

This research has been done in collaboration with Dr. Patrick L. Holland and research group, an experimental group from the University of Rochester. The research in this dissertation describes my computational efforts as part of this theory-experiment collaboration.

In this research, density functional theory was used to determine the effect of the spin state and coordination number of iron on the reaction coordinate for carbon-hydrogen bond activation by Fe(III)-(β-diketiminate)-imido complexes. These calculations were performed on both experimental models (proposed by Holland *et al.*) and computational models. Calculations indicate that for a 3-coordinate Fe-imido complex, a quartet spin state is the ground state. In the case of 4-coordinate Fe-imido complexes quartet and sextet spin states are very close in energy. The calculations further support the experimental proposal[78] by Holland *et al.* that the four-coordinate Fe^{III}-imido is the active species for C-H bond scission, and suggest a possible reason for this surprising conclusion.

CHAPTER 2

COMPUTATIONAL METHODS

In this research a large variety of computational methods have been used to determine the structural and chemical properties of various organic, inorganic and organometallic complexes. In order to determine various properties for different target species of different sizes, several levels of theory have been employed. These methods vary from simpler molecular mechanics techniques for conformational searching to more time consuming quantum mechanical techniques for geometry optimization of large molecules.

2.1 Introduction to Computational Chemistry

Electronic structure theory is the application of quantum mechanics to calculate the structure and properties of molecules. Applying the principles of quantum mechanics to molecular properties is challenging in terms of exactly solving the Schrödinger wave equation (SWE). To solve the SWE approximately, various theoretical models have been developed. Understanding the strengths and weakness of these methods is the key for applications on target molecules. Determining factors in the choice of method include the size of the molecules under study, and available computational resources.

2.2 Molecular Mechanics Method

Molecular mechanics (MM) calculates properties of target species as a function of nuclear position.[15] By neglecting the momentum and position of the electrons, the atoms' motion can be described by classical physics. These approximations make

calculations with MM much faster and less expensive than quantum mechanics (QM) based methods.

In MM, parameters are precisely defined for each type of atom based on its hybridization and coordination number. Force field parameters are used to calculate the total energy of the molecule as a sum of bond stretching, bond torsion, angle bending, electrostatic, and van der Waals interactions. In this research MM-based conformational searching has been done for species with a large number of potential conformations, i.e., complexes with many rotatable bonds. The conformations thus obtained are then refined at higher levels of theory.

2.3 Semi Empirical Methods

Semi empirical quantum mechanics (SEQM) methods use less number of parameters than MM methods. Moreover, SEQM methods consider only valence electrons and neglect many electron-electron interaction integrals deemed to be small in magnitude. Because of these reasons, SEQM methods are much faster than *ab initio* levels of theory (including DFT), but slower than MM techniques. The expected computational trade off is greater accuracy for SEQM versus MM techniques.

Among several SEQM methods, PM3(tm) (parameterization method 3 for transition metals) is employed in this research. The PM3 (tm) method uses a minimal valance basis sets of Slater type orbitals.[16] Initially, Stewart developed PM3 parameters for most elements except the transition metals,[17] and later the parameters were extended to transition metals and this method termed PM3(tm).[18]

2.4 *Ab Initio* Methods

Ab initio electronic structure methods employ the laws of quantum mechanics to solve the Schrödinger wave equation. Although many mathematical approximations are applied, finding an exact solution for the SWE equation is computationally impossible for most systems. Hartree Fock (HF) and density functional theory (DFT) are the two most important approaches developed for molecular systems.

2.4.1 Density Functional Theory

Density functional theory (DFT)[19] is currently the most widely utilized approach in electronic structure theory of transition metals. Hohenberg and Kohn originally developed this theory.[20] Their theory states that the energy of a system can be derived from its electron density. In other words, for a given set of nuclear coordinates, the electron density uniquely determines the energy and all properties of the ground state of a molecule. The applications and advantages of DFT methods are numerous.[19] The accuracy achieved by DFT calculations is often comparable to more expensive post-Hartree-Fock methods, while the computational costs are comparable to Hartree-Fock calculations.

The total energy, derived from the solution of the Schrödinger equation is the sum of kinetic energy, T, electron-nuclear attraction, V_{en}, and electron-electron interactions (the nuclear-nuclear repulsion energy is constant for a given geometry), V_{ee}. Electron-electron interaction consists of the classical Columbic repulsion (J) and non-classical terms due to the electron correlation and exchange effects.

The Kohn-Sham formulation of DFT (KS-DFT) uses the kinetic energy of non-interacting electrons, which can be solved exactly. The energy difference between real and non-interacting systems is included in the exchange correlation functional.[21]

Since the exact functionals for DFT exchange and correlation functionals are known only for a free electron gas, approximations such as the local density approximation (LDA) and generalized gradient approximation (GGA)[22] are used for molecular calculations. An LDA functional depends only on the density at the coordinates where the functional is evaluated. Although GGA is local (like LDA) it also considers the gradient of the density and hence GGA functionals are considered to be more accurate than LDA functionals.

Based on the combination of exchange and correlation functionals used either a `pure' or a `hybrid' DFT is obtained. `Pure' DFT functionals results when just exchange and correlation functionals are combined. 'Hybrid' DFT functionals result when HF exchange is added to the local DFT exchange terms. In this research, the hybrid B3LYP Hamiltonian is the DFT method of choice and the following table shows the exchange and correlation functionals used in the B3LYP model.

Table 2.1. B3LYP Exchange and Correlation Functionals

DFT MODEL	FUNCTIONALS			
	LOCAL EXCHANGE	NON-LOCAL EXCHANGE	LOCAL CORRELATION	NON-LOCAL CORRELATION
B3LYP	Slater[23] + Hartree-Fock	Becke88[24]	Vokso, Nusair, Wilk[25] + Lee, Yang, Parr[26]	Lee, Yang, Parr[25]

The methods discussed are used in the evaluation of the electronic energy for fixed nuclear positions as well as in the construction of potential energy surfaces (PESs). Gradient-based geometry optimization techniques are used to obtain stationary points on the PESs. Vibrational frequency calculations characterize the nature of the stationary points as minima (no imaginary frequency) or transition state (one imaginary frequency), and the frequencies thus obtained are used to calculate enthalpies and free energies.

2.5 Hybrid Methods

Hybrid methods combine two or more disparate levels of theory, each applied to specific regions of the chemical species of interest. In this research bulky molecules with many atoms are investigated using QM/MM methods. The ONIOM[27] (our n-layered integrated molecular orbital + molecular mechanics) QM/MM methodology has been employed. The central transition metal, atoms attached to the metal, or atoms in conjugation with these are modeled with QM techniques. The remaining atoms in the complex, typically far from the transiton metal (or reaction center), are treated with MM force fields.

2.6 Basis Sets

Basis sets are mathematical functions that describe the motion and position of electrons. In modern computational chemistry, quantum chemical calculations are typically performed with a finite set of basis functions, centered at each atomic nucleus within the molecule. These basis functions are typically Gaussian-type orbitals (GTO) due to computational considerations.

To make transition metal calculations less expensive, an approach whereby the core electrons are replaced by an average potential, the effective core potential (ECP),[28] has been utilized. Since the core electrons are minimally effected by changes in chemical bonding, ECPs reduce the number of electrons to be included in the the calculations without sacrificing much chemical accuracy. Additionally, by replacing core electrons with an ECP, scalar relativistic effects can be incorporated. The most frequently used ECP basis set in this research is CEP-31G[29] (compact effective potential, double zeta with 3 contracted and 1 uncontracted set of primitive Gaussians). The CEP-31G[28] valence basis set uses a double-zeta description for hydrogen and main group elements; single-zeta for outer core orbitals (*n*s and *n*p orbitals) of a transition metal and is triple-zeta for the metal's valence orbitals (*i.e., n*d*, (n+1)*s *and (n+1)*p *orbitals*).

The Gaussian[30] ('98 and '03 versions) programs are used for the majority of calculations described in this research.

CHAPTER 3

CARBON-HYDROGEN AND CARBON-HETEROATOM BOND ACTIVATION USING IRIDIUM (I) COMPLEXES[8,†]

3.1 Introduction

Iridium complexes with their variable formal oxidation states from –1 to +6 have played a prominent role in organometallics and homogenous catalysis. For example, the first homogeneous complex to conclusively display oxidative addition behavior was Vaska's complex – $Ir(PPh_3)_2(CO)(Cl)$.[5] Oxidation-reduction reactions of iridium complexes are of interest in terms of theoretical[31] and experimental[32] aspects. Functionalization of C-H bonds (as required in many organic synthetic transformations) requires activation of C-H bonds, and can be effected through oxidative addition by low-valent complexes of the late transition metals like iridium. Selective C-H bond activation and functionalization remains a difficult task, although considerable progress has been made.[1] Oxidative addition involving carbon-halogen bonds is of interest because of their use in many different metal-catalyzed organic syntheses starting from aryl-halides.[33] Activation of carbon-halogen bonds is also relevant to the destruction of organochlorine pollutants such as polychlorinated biphenyls.[34] The activation enthalpies for oxidative addition reactions Vaska's complex[5] with alkyl halides show larger values for carbon-heterogroup than for carbon-hydrogen bonds, which has been attributed to a polar asymmetric transition state.[35] When compared to the above reactions, oxidative addition reactions of C-O, C-N, C-S, C-P have received much less attention,[36]

† The research described in this chapter has been published originally in the journal, *Inorganica Chimica Acta*[9], and is used here with permission from Elsevier.

but they are of interest in regards to bioorganic applications like C-P bond cleavage of glycerolipids and sphingolipids.[37] Additionally, C-P bond cleavage is relevant to the degradation of phosphine-containing industrial catalysts.[38]

Oxidative addition to a singlet metal complex generally requires that the metal be stable in oxidation states separated by two units. Oxidative addition and its microscopic reverse reductive elimination[39] are in principle reversible, although for specific metal systems either one or the other is preferred. Late transition metals (like iridium) form relatively strong metal-ligand bonds, and thus tend to prefer oxidative addition.[40] Agostic complexes with C-H···M and C-X···M bridges have been of interest since they were first characterized.[41] They can be thought of as modeling intermediate species on the reaction pathway for oxidative addition. How such agostic intermediates compete when there is a potential donor group on the substrate has not been investigated. In the current research the kinetics and thermodynamics of oxidative addition/reductive elimination will be studied for a variety of C-X (X = H, N, O, F, P, S, Cl) bonds.

3.2 Computational Methods

The first step in any computational study is to determine reasonable geometries for target molecules. Since experimental techniques like X-ray crystallography are limited to stable materials with appreciable life times, progress in computational methods and technology has resulted in an explosion in the use of modeling for the analysis of chemical processes and materials, and in the determination of transition states.

The Gaussian 98 package was used for this research. The exchange functional proposed by Becke[23] was employed along with the gradient-corrected correlation functional of Lee, Yang and Parr.[25] Becke's three parameter functional (B3), a hybrid functional, defines the exchange functional as a linear combination of Hartree Fock, local and gradient-corrected exchange terms. The basis set for iridium and all main group elements was the effective core potential (ECP) valence basis set of Stephens, Basch, and Krauss[28] (CEP-31G) augmented with d-polarization functions for main group elements with corresponding exponents of 0.8 for carbon, nitrogen and fluorine, 0.55 for phosphorus, 0.65 for sulfur, and 0.75 for chlorine. This level of theory has been employed in numerous previous studies and shown to be reliable for the prediction of transition metal geometries, energetics, and spectral properties as long as used in conjunction with a suitable wavefunction or density functional technique.[42]

Reactant, transition state and product geometries were fully optimized using gradient methods. The geometry optimization was performed on singlet multiplicities without constraint of symmetry. The energy Hessian was calculated and thus confirmed the stationary points as minima (no imaginary frequencies) or transition states (one imaginary frequency) as appropriate. Reported enthalpies and entropies at 1 atm and 298.15 K were calculated using B3LYP/CEP-31G(d) determined frequencies.

3.3 Results and Discussion

3.3.1 Geometries of Products, $Ir(PH_3)_2(CH_2X)(H)_2$ and $Ir(PH_3)_2(H)(X)(CH_3)$

The first goal of this research was to determine an appropriate geometry for the isomeric five-coordinate oxidative addition products, $Ir(PH_3)_2(CH_2X)(H)_2$ and

$Ir(PH_3)_2(H)(X)(CH_3)$. The former results from the C-H activation pathway, equation 1, while the latter product arises from C-X activation, equation 2. Based on experimental models, it was assumed that the phosphine ligands

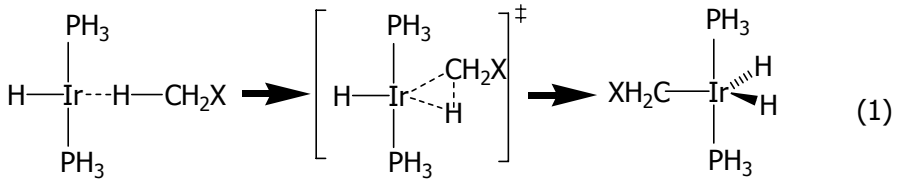

(1)

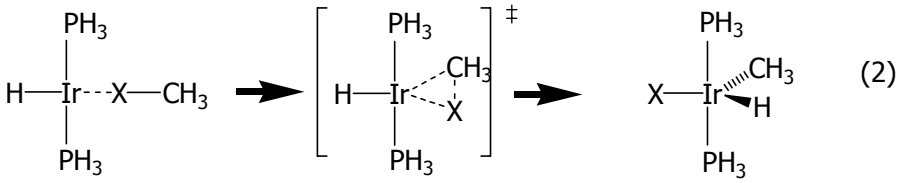

(2)

X = F, Cl, OH, SH, NH_2, PH_2

remain *trans* to each other. Geometry optimization of assumed trigonal bipyramidal and square pyramidal structures for product models at the B3LYP/CEP-31G(d) level of theory lead to stable structures with the heteroatom (X) or heteroatom-containing (CH_2X) group at the base of a Y-shape minimum (*i.e.*, one acute plus two obtuse ligand-metal-ligand angles for the three equatorial ligands of a distorted trigonal bipyramid) for both C-X and C-H activation. The exception is the product of C-H activation of CH_3F, which yields a Y-shaped minimum $Ir(PH_3)_2(H)_2(CH_2F)$ with the H at the base. Riehl *et al.* have discussed the structure of d^6-Ir(III) species and the calculated geometries obtained in this research are consistent with their conclusions.[43] The average bond angles for the C-X activation products, $Ir(PH_3)_2(H)(X)(CH_3)$, change very little with the change in X group: X-Ir-CH_3 = 141 $\pm$ 2°, X-Ir-H = 144 $\pm$ 1°, and H-Ir-CH_3 = 74 $\pm$ 1°, Table 3.1. For the C-H activation product, $Ir(PH_3)_2(X)(CH_3)(H)$, the ligand-metal-ligand angles are more variable, Table 1. This is due in part to the

observation that some of the X groups, most notably amino (NH_2) and chloro (Cl), of the heteromethyl (CH_2X) ligand participate in bonding to the Ir. Comparison of bond measurements of target molecules, Table 1, with experimental models from the Cambridge Structural Database (CSD)[44] shows considerable proximity between calculated and experimental metal-ligand bond lengths (n is sample size): Ir-F = 2.04 Å (calcd.; 2.01 ± 0.11 Å, n = 7, expt.), Ir-OH = 2.04 Å (calcd.; 2.04 ± 0.03 Å, n = 5, expt.[1]), Ir-NH_2 = 2.00 Å (calcd.), Ir-Cl = 2.44 Å (calcd.; 2.41 ± 0.06 Å, n = 594, expt.), Ir-SH = 2.38 Å (calcd., 2.40 ± 0.03 Å, n = 4), Ir-PH_2 = 2.41 Å (calcd.; Ir-PR_2 = 2.30 Å for JOHWIM[20]); Ir-C(sp^3)=2.12 $\pm$ 0.02 (calcd.; 2.13 $\pm$ 0.07 Å, n = 380), Ir-PR_3 = 2.26 $\pm$ 0.01 Å (calcd., 2.32 $\pm$ 0.05 Å, n = 685), Ir–H = 1.61 $\pm$ 0.04Å (calcd.; 1.59 $\pm$ 0.17 Å, n = 248).

Table 3.1. Calculated Metric Data for Adduct Ir (I) React and Five-Coordinate Products[a]

C-X Activation Reactant, Adduct [Ir]…X-CH_3

X	Ir…X-C	X…Ir-H	Ir-X	Ir-H	Ir-PH_3	C-X
F	116	178	2.50	1.57	2.25	1.42
Cl	108	179	2.59	1.59	2.26	1.83
OH	120	176	2.33	1.59	2.25	1.45
NH_2	116	180	2.24	1.61	2.26	1.85
SH	110	178	2.41	1.62	2.25	1.49
PH_2	118	179	2.31	1.65	2.26	1.86

C-X Activation Product [Ir](CH_3)X

X	X-Ir-CH_3	X-Ir-H	H-Ir-CH_3	Ir-X	Ir-Me	Ir-H
F	143	145	73	2.04	2.11	1.57
Cl	143	143	75	2.44	2.11	1.59
OH	141	146	73	2.04	2.12	1.59
NH_2	140	146	74	2.00	2.14	1.60
SH	140	144	75	2.38	2.12	1.59
PH_2	139	147	74	2.41	2.14	1.59

[1] This estimate includes Ir-OH and Ir-OMe complexes.

C-H Activation Reactant, Adduct [Ir]…H-CH_2X[c]

X	H_1-Ir…H_a	Ir…H_a-C	Ir….H_aC	Ir-H_1	C-H_a
F	162	115	2.03	1.57	1.13
Cl	160	120	2.09	1.57	1.12
OH	163	120	2.00	1.57	1.14
NH_2	160	113	2.07	1.57	1.11
SH	160	115	2.06	1.57	1.10
PH_2	161	116	2.06	1.57	1.10

C-H Activation Product [Ir](CH_2X)H

X	H_1-Ir-CH_2X	H_1-Ir-H_2	H2-Ir-CH_2X	Ir-H_1	Ir-CH_2X	Ir-H_2
F	75	130	154	1.57	2.10	1.71
Cl	111	82	166	1.57	2.12	1.66
OH	146	63	150	1.58	2.15	1.62
NH_2	117	87	156	1.57	2.14	1.66
SH	146	65	148	1.57	2.18	1.60
PH_2	150	65	146	1.57	2.18	1.66

[a] Bond lengths in Angstrom and bond angles in degrees.
[b] [Ir] ≡ Ir(PH_3)$_2$(H)
[c] H_a is the agostic hydrogen

3.3.2 Reactant (Adduct) Geometries, (PH_3)$_2$(H)Ir ···H-CH_2X and (PH_3)$_2$(H)Ir ···X-CH_3

There is initial formation of an adduct between the activating complex, Ir(PH_3)$_2$H, and the substrate CH_3X.[45] Adducts were isolated by distorting the oxidative addition transition states (*vide infra)* along the reaction coordinate toward their respective reactants, which was then followed by geometry optimization. Two isomeric minima are found for these square planar Ir(I) species, one in which the substrate coordinates agostically through the C-H bond, and the other in which the substrate coordinates through its heteroatom. The iridium-heteroatom interactions for adducts on the C-X activation pathway range from relatively weak Ir···X interactions for the methyl halides (X = Cl, F) to more substantially bound donor-acceptor complexes for the other

heteroatom groups. Binding enthalpies for adducts were not corrected for basis set superposition error, although this is expected to impact the absolute binding enthalpies more so than the relative binding energies. In general, the X-ligated adduct is more stable than the agostic Ir···H-C isomer: $\Delta\Delta H$(CH-CX) = 0 (F); 6 (OH); 17 (NH_2); 5 (Cl); 16 (SH); 30 (PH_2) kcal/mol. In a previous study, Hall *et al.* found $(CO)_5W\cdots F\text{-}CH_3$ to be substantially more strongly bound than $(CO)_5W\cdots H\text{-}CH_2F$.[46] Therefore, it is interesting to note that there is a near degeneracy of the $Ir\cdots F\text{-}CH_3$ and $Ir\cdots H\text{-}CH_2F$ adducts.

The calculated adduct binding enthalpies range from –3 (X = Cl) to –5 (X = OH) kcal/mol for the agostic Ir···H-C adducts. Hence, it does not appear that heteroatom substitution greatly affects the energetics of M···H-C agostic interaction. As expected, the Ir···X-C adducts show greater variability in adduct binding enthalpies: -4 (F), -11 (OH), -22 (NH_2), -8 (Cl), -20 (SH), -34 (PH_2) kcal/mol. The trends in binding enthalpies show the group 15 donors to be more strongly bound than the group 16 donors, which are in turn more strongly bound than the halogen donors. Additionally, the binding enthalpy of the heavier donors (X = P, S, Cl) are greater than that of their lighter congeners, a result consistent with simple hard-soft, acid-base concepts.

3.3.3 Transition States for C-X and C-H Activation

Calculations indicate a three-center transition state (TS) with *trans* phosphine ligands. B3LYP/CEP-31G(d) energy Hessian calculations, yielding a single imaginary frequency, confirm these geometries as first order saddle points. The imaginary frequency is more constant in the transition states for C-H activation (TS_H, ν_i = 820 ±

21 cm^{-1}) and more variable for the C-X bond activation transition states (TS_X, X = F, 546i cm^{-1}; Cl, 432i cm^{-1}; OH, 533i cm^{-1}; SH, 400i cm^{-1}; NH_2, 504i cm^{-1}; PH_2, 349i cm^{-1}). The single imaginary frequency is characterized by C-H (or C-X) bond formation/scission for the substrate bond being activated.

Comparison of the iridium-carbon bond lengths in Table 3.1 and Table 3.2 shows a ≈5% increase in the iridium-carbon bond length for TS_H relative to the product $Ir(PH_3)_2(H)_2(CH_2X)$ and ≈14% increase in the Ir-C bond length for TS_X relative to the C-X activation product $Ir(PH_3)_2(X)(CH_3)(H)$. These data suggest a relatively late transition state for both C-H and C-X oxidative addition. Furthermore, the metric data suggest that the transition states for C-H activation are later on their respective potential energy surfaces than the corresponding C-X activation transition states.

Table 3.2. Transition State Geometries for C-H and C-X Bond Activation[a]

C-X Oxidative Addition Transition State:

X	X…Ir…Me	X…Ir-H	H-Ir…CH_3	Ir…X	Ir…Me	Ir-H	Me…X
F	43	173	130	2.21	2.51	1.59	1.77
Cl	49	178	129	2.53	2.67	1.60	2.15
OH	47	175	129	2.19	2.40	1.61	1.84
NH_2	53	176	124	2.10	2.32	1.63	2.19
SH	53	177	128	2.42	2.27	1.62	1.97
PH_2	57	131	171	2.31	2.39	1.61	2.24

C-H oxidative Addition Transition State:

X	H_1-Ir…C	H_1-Ir…H_2	H_2…Ir…C	Ir…H_1	Ir…C	C-H	Ir-H_2
F	165	154	41	1.65	2.24	1.48	1.63
Cl	167	151	41	1.64	2.25	1.49	1.63
OH	163	154	42	1.65	2.27	1.54	1.63
NH_2	164	152	43	1.65	2.26	1.53	1.63
SH	168	149	42	1.64	2.27	1.55	1.62
PH_2	168	148	43	1.65	2.28	1.57	1.62

[a] Bond lengths in Angstrom units and bond angles in degrees.

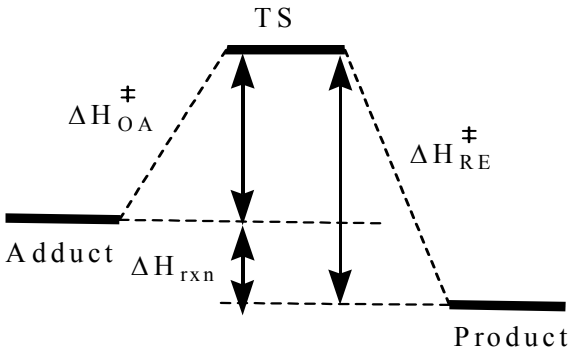

Scheme 3.1

3.4 Thermochemistry

The calculated enthalpic quantities of interest are depicted in Scheme 3.1. These include the barrier to oxidative addition ($\Delta H_{OA}^{\ddagger}$, adduct → TS), the barrier to reductive elimination ($\Delta H_{RE}^{\ddagger}$, product → TS), and the enthalpy of reaction (ΔH_{rxn}, reactant → product).

The C-H oxidative addition reactions (adduct → five-coordinate product) are close to thermoneutral for all substituents. The only two systems that are significantly different are X = NH_2 and Cl, whose reactions are substantially more exothermic (ΔH_{rxn} < -8 kcal/mol) than for the other substituents. As mentioned above, the geometries for $Ir(PH_3)_2(H)_2(CH_2Cl)$ and $Ir(PH_3)_2(H)_2(CH_2NH_2)$ predicted an interaction between iridium metal and the X group of the heteromethyl ligand that is not present in other products, Figure 3.1. Attempts to manually construct conformers with metal/pendant X group interactions for the other heteroatoms resulted in geometries that either reverted back to the original conformations, or higher energy conformers. Product stabilization by pendant X group – metal interaction results in a larger reductive elimination barrier (five coordinate product → TS_H) for chloro and amino substituted models ($\Delta H_{RE}^{\ddagger}$ = 16.0 and

16.2 kcal/mol, respectively) relative to other substituents ($\Delta H_{RE}^{\ddagger} \leq 13$ kcal/mol) since Ir···X interaction is not evident in the transition states for these substrates.

Inspection of the data in Table 3.3 shows interesting trends in terms of the kinetics of C-H oxidative addition. For the calculated oxidative addition barriers

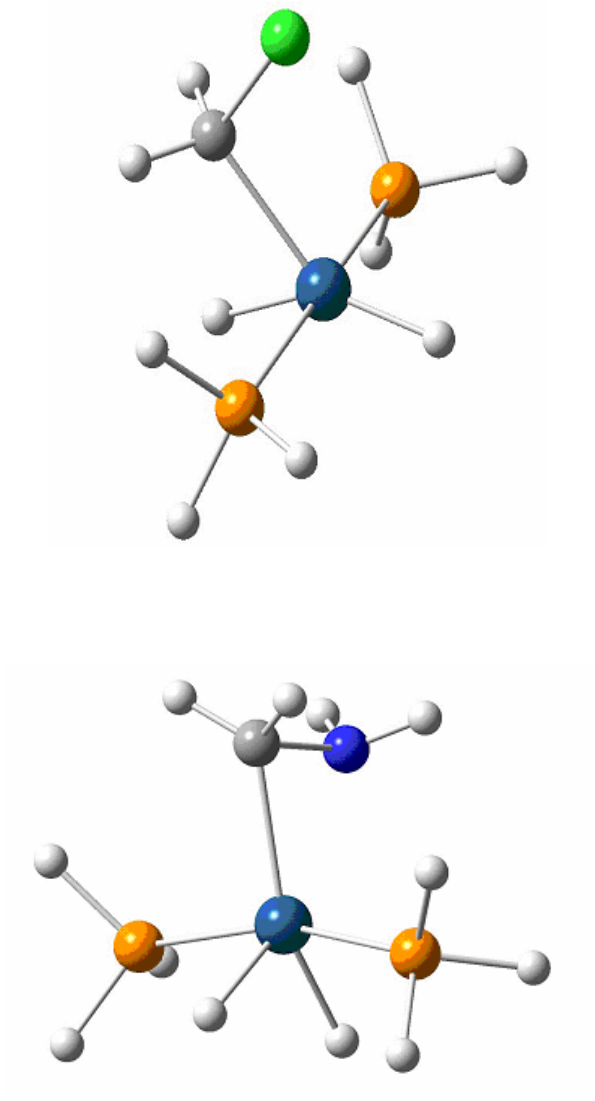

Figure 3.1. Products of C-X activation of H_3C—Cl (top) and H_3C—NH_2 (bottom) showing interaction between heteroatom and iridium.

($\Delta H_{OA}^{\ddagger}$, Scheme 3.1) of the C-H bond of CH_3X to $Ir(PH_3)_2H$ it is observed that F < OH < NH_2, and Cl < SH < PH_2. Additionally, the heavy atom substituents (X = Cl, SH, PH_2) are higher than their corresponding light atom substituents (X = F, OH, NH_2), Table 3.3. These data immediately suggests a correlation between Pauling electronegativities and $\Delta H_{OA}^{\ddagger}$. Previous calculations[45] indicate that the dominant interaction late in the reaction coordinate of C-H oxidative addition is metal $d\pi \rightarrow$ CH σ^* backbonding. One may propose that a more electronegative X substituent will stabilize the CH σ^* through inductive effects, making it a better acceptor and facilitating C-H scission. Support for this contention comes from reasonable linear correlations ($R \geq 0.9$) between calculated CH oxidative addition barriers, Table 3.3, and Pauling electronegativities (F, 4.0; Cl, 3.5; O, 3.5; S, 2.5; N, 3.0; P, 2.1), and NBO (Natural Bond Order[47]) determined energies for σ_{CH}^* for CH_3X (F, 0.505 a.u.; OH, 0.515 a.u.; NH_2, 0.542 a.u.; Cl, 0.524 a.u.; SH, 0.536 a.u.; PH_2, 0.541 a.u.).

As with the C-H activation energetics, interesting trends in the thermodynamics and kinetics of C-X activation as a function of X are seen. Not surprisingly, the variations are more substantial when the heteroatom is a direct participant in the oxidative addition process. The enthalpy of the reaction (adduct $\rightarrow$ five coordinate product) becomes less endothermic for both light and heavy element groups in the order group 17 < group 16 < group 15. All C-X oxidative additions are exothermic, except for X = amino (ΔH_{rxn} = +3.3 kcal/mol) and phosphino (ΔH_{rxn} = +14.9 kcal/mol). The reductive elimination barriers to form CH_3X from $Ir(PH_3)_2(H)(X)(CH_3)$ are very large and all in the range 41 – 53 kcal/mol, except for X = PH_2 ($\Delta H_{RE}^{\ddagger}$ = 21.7 kcal/mol).

In light of the success in interpreting trends in C-H oxidative addition barriers using Pauling electronegativities and the NBO derived energy of the acceptor orbital (σ^*_{CX} in the present case), a similar analysis was performed for C-X oxidative addition. A poor linear correlation ($R \sim -0.38$) is found between the Pauling electronegativity of X and $\Delta H_{OA}^{\ddagger}$, but a much stronger correlation ($R \sim 0.94$) between $\varepsilon_{\sigma^*(CX)}$ and $\Delta H_{OA}^{\ddagger}$. The positive sign of the correlation coefficient indicates that a lower energy σ^*_{CX} (*i.e.*, a better acceptor) yields a lower oxidative addition barrier.

Table 3.3. Calculated Enthalpies (in a.u.) and Enthalpic Barriers (kcal/mol) for C-X and C-H Activation

C-X Activation

X	Adduct	TS	Product	$\Delta H_{RE}^{\ddagger}$	$\Delta H_{OA}^{\ddagger}$	ΔH_{rxn}
F	-153.6353	-153.5933	-153.6732	50.1	26.4	-23.7
OH	-146.0173	-145.9622	-146.0337	44.9	34.5	-10.3
NH_2	-140.5539	-140.4826	-140.5486	41.4	44.8	3.3
Cl	-144.3875	-144.3576	-144.4417	52.8	18.8	-34.0
SH	-140.2154	-140.1719	-140.2392	42.2	27.3	-14.9
PH_2	-137.2033	-137.1450	-137.1795	21.7	36.5	14.9

C-H Activation

X	Adduct	TS	Product	$\Delta H_{RE}^{\ddagger}$	$\Delta H_{OA}^{\ddagger}$	ΔH_{rxn}
F	-153.6353	-153.6260	-153.6392	8.2	5.8	-2.4
OH	-146.0072	-145.9948	-146.0091	9.0	7.8	-1.2
NH_2	-140.5272	-140.5121	-140.5379	16.2	9.5	-6.7
Cl	-144.3803	-144.3689	-144.3944	16.0	7.1	-8.9
SH	-140.1901	-140.1749	-140.1958	13.1	9.6	-3.6
PH_2	-137.1551	-137.1374	-137.1517	8.9	11.1	2.2

3.5 Summary and Conclusions

A major motivation for this research is to compare the reaction coordinates for C-H activation versus C-X activation in order to address issues of kinetic (transition state)

and thermodynamic (ground state) selectivity. To this end, Table 3.4 organizes the calculated relative enthalpies of the various isomeric stationary points for C-H and C-X activation.

Table 3.4. Relative Enthalpies (in kcal/mol) of C-H and C-X Activation[a]

	Adduct	TS	Product
F-H	23.8	29.6	21.3
F-X	23.7	50.1	-0-
OH-H	16.6	24.4	15.4
OH-X	10.3	44.9	-0-
NH_2-H	16.7	26.2	10
NH_2-X	-0-	44.8	3.3
Cl-H	38.5	45.7	29.7
Cl-X	34	52.8	-0-
SH-H	30.8	40.3	27.2
SH-X	14.9	42.2	-0-
PH_2-H	30.2	41.3	32.4
PH_2-X	-0-	36.5	14.9

[a] Values are relative to the lowest energy stationary point for a given X group (designated by -0-).

For adducts, except in the case of X = F, the X-ligated adduct is substantially more stable than the Ir···H-C agostic adduct. This is not surprising since the X group is expected to be a substantially better donor than a σ_{CH} orbital, and the early portion of the oxidative addition reaction coordinate is dominated by substrate to complex donation. Additionally, substituents are found to have little effect on the strength of Ir···H-C agostic bonding.

For products, the C-H and C-X oxidative addition result in Y-shaped, Ir(III) products with geometries that are in good agreement with experimental estimates as discussed above. Oxidative addition of C-H bonds to form the C-H addition product is close to thermoneutral for all X groups studied. However, additional stabilization of the

product was found in the case of substrates (X = Cl, NH_2) for which the α-X substituent displayed some interaction with the iridium. Oxidative addition of the C-X bond to form $Ir(PH_3)_2(H)(CH_3)(X)$ was exothermic for X substituents from groups 16 and 17, but endothermic for group 15 (X = NH_2, PH_2) substituents. Additionally, the enthalpy of reductive elimination from the C-X products was substantially greater than the enthalpy of C-H reductive elimination. Taken together, the product of C-X activation $Ir(PH_3)_2(H)(CH_3)(X)$ is significantly lower in enthalpy than the corresponding C-H activation product $Ir(PH_3)_2(H)_2(CH_2X)$ by between 7 (X = NH_2) and 30 (X = Cl) kcal/mol, Table 3.4. It seems reasonable to infer that the preference for $Ir(PH_3)_2(H)(CH_3)(X)$ over $Ir(PH_3)_2(H)_2(CH_2X)$ is due to the lower bond energy of C-H relative to C-X (with the exception of X = F) and greater Ir-X than Ir-H bond energies. Hence, overall there is a significant thermodynamic preference for C-X activation by these Ir(I) complexes.

The transition states for both C-H and C-X oxidative addition can be labeled as late or product-like. The Ir-C and Ir-H (or Ir-X) bonds in the transition states are slightly longer than the values they assume in the product. Analysis of the Ir---C bonds common to both TSs suggests that the C-H activation TSs are later than their corresponding C-H activation transition states. This is reasonable given that C-H oxidative addition is generally less exothermic/more endothermic than C-X oxidative addition.

The C-H activation TSs are substantially lower than their C-X activation counterparts, Table 3.4. For X = F, OH, NH_2, the kinetic advantage for C-H activation is substantial, being greater than 18 kcal/mol for all three substituents. For the heavy

element substituents, C-H and C-X bond activation are more competitive in a kinetic sense. Indeed, for X = PH_2, the C-X activation TS is *lower* than the corresponding C-H activation barrier for CH_3PH_2. This is indeed interesting given the potential degradation pathways in industrially important phosphine coligands. Hence, in the competitive activation of C-H and C-X bonds of CH_3X by $Ir(PH_3)_2(H)$ by way of an oxidative addition pathway, we see a dichotomy. There is a thermodynamic preference for C-X activation, but a kinetic preference for C-H activation.

CHAPTER 4

THEORETICAL STUDY OF GROUP TRANSFER FROM MULTIPLY BONDED NICKEL COMPLEXES TO ETHYLENE.[48†]

4.1 Introduction

Formation of carbon-carbon and carbon-heteroatom bonds is a fundamental purpose in synthetic organic chemistry.[49] Atom and group transfer reactions mediated by transition metal centers represent a prominent area of current research as these reactions are central to the chemistry of transition metal complexes with multiply bonded ligands.[50] Such process is finding relevance in the field of catalysis, and also has been widely proposed in catalytic processes that occur in metalloprotein active sites. For example, biological oxygen atom transfer reactions to organic substrates, catalyzed by metalloenzymes and their biomimetics, are well known.[51]

Due to the presence of filled $d\pi$ orbital, very few examples of multiply bonded complexes of the late transition metals such as cobalt, nickel and copper are known.[52] Examples of multiply bonded transition metal complexes are typically limited to metals from the early to middle transition series in high formal oxidation states.[53] The majority of terminal oxo complexes have d^{0-2} configurations,[54] which therefore does not result in occupation of metal-ligand π^* orbitals for the most common octahedral and square pyramidal coordination geometries. Synthesis of multiply-bonded nickel complexes with phosphinidene,[11] carbene[12] and nitrene[13] ligands by Hillhouse and his group are rare examples of stable multiply bonded complexes of the late transition metals.

---

†The research described in this chapter has been accepted for publication originally in the journal, *THEOCHEM*,[48] and is used here with permission from Elsevier.

Furthermore, these complexes have been used for organic synthetic transformations, specifically group transfer to olefins to form three-membered ring products.[11,12,13]

Aziridines serve as important intermediates for functional group modifications and ligands in asymmetric catalysis; their synthesis has thus been a subject of considerable interest. Evans[55] and Jacobsen,[56] among others, have done important work on transition metal-catalyzed aziridination. For example, they reported that Cu(I) and Cu(II) salts form competent precatalysts and indicated that a common oxidation state is reached in both cases.[53,54] Brandt *et al.,* performed a combination of hybrid density functional (B3LYP) calculations and kinetic experiments[57] on Cu(I) and Cu(III) complexes and proposed a catalytic cycle to demonstrate the inactivity of the higher oxidation state of copper for aziridination. Recent preparations of metastable Ni-nitrene complexes by Hillhouse *et al.*[13] have allowed their aziridination reactivity to be directly assessed. These researchers reported the stoichiometric transfer of nitrene fragments to ethylene resulting in the formation of aziridines.

Cyclopropanes are also an important class of molecules. The strain associated with the three-membered ring allows cyclopropanes to undergo useful ring-opening reactions in organic synthesis. The Simmons-Smith reaction using zinc is a classic method for the synthesis of cyclopropanes from olefins[58] for which a carbenoid intermediate is proposed.

The chemistry of phosphorus-containing, three-membered ring compounds has not been studied as extensively as their oxygen, nitrogen, or carbon congeners.[59] Since the early studies of phosphiranes by Wagner[60] and Chan,[61] several synthetic

approaches have been developed. Phosphiranes were not studied in much detail until Mathey and co-workers developed improved synthetic methods via Cr-triad complexes.[62] Phosphiranes have several interesting properties. Compared to normal phosphines their resistance to oxidation is the noteworthy. Monocyclic phosphiranes tend to form metallaphosphetanes with electron-rich metals via an insertion of the metal center into a σ_{PC} bond.[63] Phosphiranes may act as better π-acceptors versus acyclic phosphines, because the pyramidalization of the phosphorus coordination sphere decreases the energy the acceptor orbitals that are σ^*_{PC} in character. Finally, a previous computational study[64] of phosphiranes indicated that they have interesting stereoelectronic properties as compared to traditional acyclic phosphines used in organometallic catalysis, and thus pathways to their synthesis are also important in this regard.

Recent preparation of stable nitrene,[13] phosphinidine[11] and carbene[12] complexes with (dtbpe)Ni (dtpbe = 1,2-*bis*(di-*tert*-butylphosphino)ethane) has expanded the study of reactivity of late transition metal multiply bonded complexes. The kinetics and thermodynamics of the proposed mechanism for the reaction of ethylene with (dhpe)Ni=E, dhpe = 1,2-*bis*(dihydrophosphino)ethane), have been studied in the present research.

4.2 Computational Methods

The Gaussian 03[29] package was used for this research. The B3LYP functional was employed.[23,25] For nickel and main group elements the effective core potential (ECP) and valence basis sets of Stephens, Basch and Krauss[28] (CEP-31G) was employed,

augmented with a d-polarization function for main group elements (exponent of 0.8 for C and N; 0.55 for P). The –31G basis set was employed for hydrogen.

All stationary points were singlets and fully geometry optimized using gradient methods without symmetry constraint. The calculated energy Hessian confirmed the stationary points as a minima (no imaginary frequency) or transition state (one imaginary frequency). The thermochemistry of the reaction was determined at 1 atm and 298.15 K using B3LYP/CEP-31G(d) determined frequencies.

4.3 Results and Discussion

The process studied is the reaction between (dhpe)Ni=E (E = CH_2, NH, PH) and two equivalents of ethylene to give cyclic organic and Ni(0)-ethylene products as shown in the following equation. Figure 4.1 shows the two-step reaction sequence proposed for the reaction 4.1. In this reaction the heterogroup is transferred to ethylene

$$(dhpe)Ni{=}E \; + \; 2\,C_2H_4 \longrightarrow \underset{H_2C-CH_2}{\overset{E}{\diagup\!\diagdown}} + (dhpe)Ni(C_2H_4) \qquad (4.1)$$

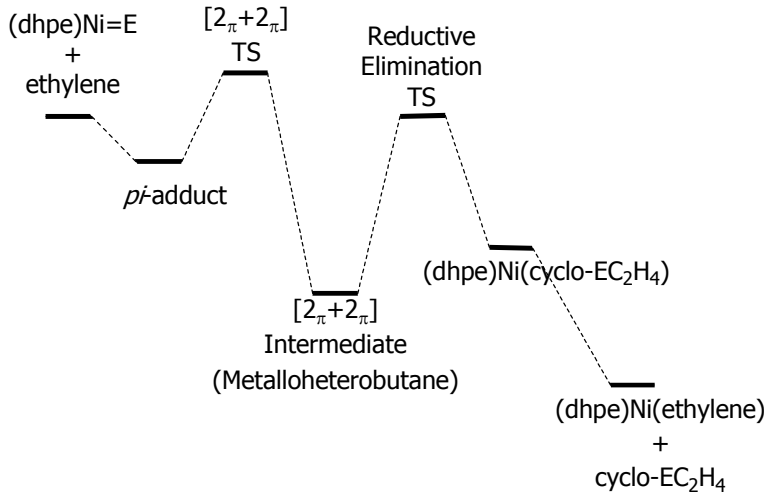

Figure 4.1. Reaction sequence for (dhpe)Ni=E and ethylene.

The first phase of the mechanism is the interaction of the Ni=E complex with an equivalent of ethylene to give a four-membered ring product through a [2_π + 2_π] mechanism. The second phase of the reaction is conversion of a metallaheterobutane through a C-E reductive elimination transition state to yield a three-membered ring product, which is then dissociated from the nickel by coordination of a second molecule of ethylene.

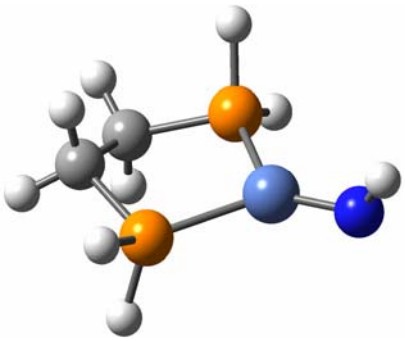

Figure 4.2. Geometric minimum of (dhpe)Ni(NH).

4.3.1 Reactants

It was found that DFT geometry optimization of (dhpe)Ni=E leads to stable, terminally bonded minima for nitrene, phosphinidene and carbene models, but not for the oxo (E = O) congener. Figure 4.2 shows the minimum obtained for (dhpe)Ni=NH, which like the phosphinidene and carbene analogues has an approximately trigonal planar coordination environment at nickel. When these calculations were extended to the isovalent Ni-oxo complex, B3LYP/CEP-31G(d) geometry optimization resulted in insertion of oxygen into a Ni-phosphino bond (Figure 4.3), suggesting the instability of (dhpe)Ni=O complexes. Hence, subsequent calculations will focus on phosphinidene, nitrene and carbene group transfer.

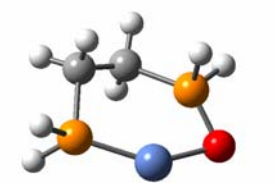

Figure 4.3. Calculated geometric minimum for "Ni-oxo" reactant.

Comparison of the bond measurements of the target models with the experimental complexes synthesized by Hillhouse *et al.*[11,12,13] showed reasonable proximity between the calculated and experimental Ni=E bond lengths bond lengths. Ni=CH_2 = 1.78 Å (calc.; 1.836(2) Å, expt.), Ni=NH = 1.69 Å (calc.; 1.702 Å, expt.), Ni=PH 2.09 Å (calc.; 2.07 Å, expt.). Similar comparisons of the P-Ni-P bite angles showed good correlation with the complexes of Hillhouse *et al.*, despite the lack of bulky *tert*-butyl groups in the models. For the (dhpe)Ni=E complex, P_1-Ni-P_2 = 88º (calc. for all E; 91º - 92º, expt.). Comparison of the average P-Ni=E angles between calculated and experimental models likewise showed good agreement: Ni-carbene, ave. P_1/P_2-Ni-C = 136º (calc.; 133º, expt.); Ni-nitrene, ave. P_1/P_2-Ni-N = 136º (calc.; 132º, expt.) and for the phosphinidene analogue, P_1/P_2-Ni-P = 136º (calc.; 132º, expt.). The Ni-P_{dhpe} bond lengths remained virtually constant for the different hetero groups ranging from 2.17 Å – 2.18 Å.

4.3.2 Ethylene Pi Adducts

Given the low coordination number of the nickel in (dhpe)Ni=E, and the π-donor capacity of olefins, there exists the possibility of initial formation of a π-adduct between the (dhpe)Ni=E and the ethylene substrate. Ethylene π-adducts were searched and isolated by distorting the [2+2] transition states (section 4.3.3) along the reaction

coordinate toward their respective reactant geometries followed by B3LYP/CEP-31G(d) geometry optimization. The calculated ethylene adduct binding enthalpies range from –3 (E = NH) to –8 (E = PH) kcal/mol. Hence, it does not appear that heteroatom substitution substantially affects the energetics of Ni←ethylene interaction. Furthermore, in the face of an unfavorable entropic contribution to ethylene binding and the greater steric bulk of dtbpe versus dhpe, the calculations imply that initial binding of ethylene to the nickel complex is very weak if extant at all in the experimental systems.

4.3.3 $[2_\pi+2_\pi]$ Transition States

Calculations indicate a four-centered, $[2_\pi+2_\pi]$ transition state (TS) connecting the reactants and a metallaheterobutane (discussed in section 4.3.4), Figure 4.4. B3LYP/CEP-31G(d) energy Hessian calculations yielding a single imaginary frequency confirmed the isolated geometries as first-order saddle points. The single imaginary frequency is characterized by substrate activation through the strengthening of Ni•••C as well C•••E bonds leading to the four-membered ring intermediate described in the next section.

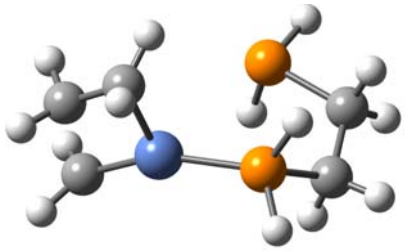

Figure 4.4. $[2_\pi+2_\pi]$ transition state for ethylene addition to (dhpe)Ni=CH_2.

Comparison of the Ni•••E bond lengths in the $[2_\pi+2_\pi]$ transition state, Table 4.1, with the NiE bond in the corresponding reactants showed an increase of 1% for E = CH_2, 2% for E = NH and 5% for E = PH. A similar comparison of Ni•••E in the TS versus the corresponding bond in the products showed an increase of 6% for E = CH_2, NH and 2% for E = PH. These comparisons suggest a relatively "early" $[2_\pi+2_\pi]$ transition state for carbene and nitrene and a somewhat later transition state for phosphinidene addition.

Table 4.1. T.S. Geometries for $[2_\pi+2_\pi]$ Addition of (dhpe)Ni=E to Ethylene[a]

E	NiE	Bite Angle	P_1NiE	P_2NiE	E-C	Ni-C	Ni-P_1	Ni-P_2
CH_2	1.84	71.2	154.1	103.6	1.95	1.91	3.49	2.13
NH	1.74	86.7	113.2	108.5	3.01	2.5	2.41	2.21
PH	2.29	68.8	102.2	93.8	1.81	1.78	3.65	2.15

[a] Bond lengths in Angstrom units; bond angles in degrees

Perhaps the most interesting result regarding the $[2_\pi+2_\pi]$ transition states is that the DFT calculations indicate that these transition states are accompanied by the dissociation of one of a Ni-phosphine bond of the dhpe ligand (see Figure 4 for carbene example). The dissociation of the Ni-P bond might be predicted to enhance the feasibility of interaction between Ni and ethylene substrate through opening of a coordination site. However, recall that the (dhpe)Ni=E(π-ethylene) minima (section 4.3.2) were obtained by distorting the $[2_\pi+2_\pi]$ transition state along the reaction coordinate, and then reoptimizing the geometry. The resulting π-adducts were found to be very weakly bound. However, one may still propose that observation of a geometric

perturbation of the Ni(dhpe) fragment from $\eta^2 \rightarrow \eta^1 \rightarrow \eta^2$ along the reaction coordinate from the (dhpe)Ni=E to the [2_π+2_π] TS to the metallaheterobutane, respectively, may engender some kinetic or regiochemical benefit for the initial step of this two-step mechanism. The energetics of the transition states will be addressed in section 4.4.

4.3.4 Four-Membered Ring [2+2] Intermediates

Distortion of the [2_π+2_π] transition state along the reaction coordinate toward products, followed by geometry optimization yielded a four-membered ring metallaheterobutane intermediate. Calculations indicate these structures to be stable geometric minima. The formation of the [2+2] intermediate is also accompanied by ring closure of the dhpe ligand back to η^2 coordination (compare Figure 4.4 and Figure 4.5). Calculations showed square planar geometry around Ni(II) center and showed good correlation of bond measurements with experimental geometries.[11,12,13]

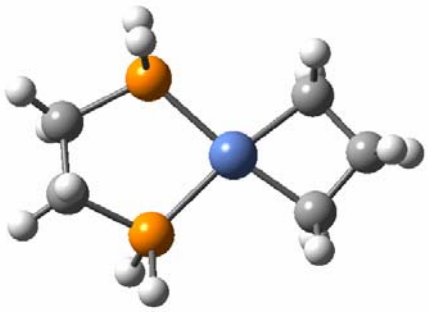

Figure 4.5. [2_π+2_π] intermediate from [2_π+2_π] transition state.

4.3.5 Reductive Elimination Transition States

The four-membered ring intermediates discussed above are followed by three-centered reductive elimination transition states that form the second E-C bond of the eventual cyclo-EC_2H_4 products, Figure 4.6. B3LYP/CEP-31G(d) energy Hessian

calculations, yielding a single imaginary frequency, confirm these geometries as first order saddle points. Stretching/compression of the Ni•••C and C•••E bonds primarily characterize the single imaginary frequency of these transition states.

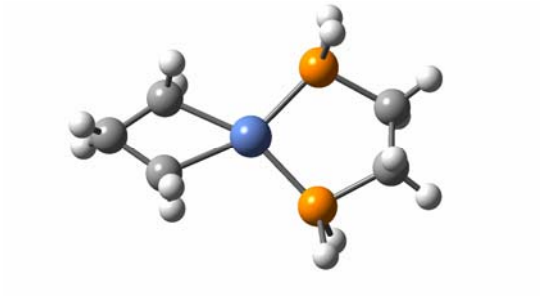

Figure 4.6. Reductive elimination transition state.

Comparison of the Ni•••E bond lengths in Table 4.2 with the corresponding bond lengths for the [2+2] intermediate shows an increase of 8% for E = CH_2, 2% for E = NH and 4% for E = PH and the comparison with NiE bond lengths in the products shows an increase of 54% for E = CH_2, 66% E = NH and 74% for E = PH. These comparisons thus suggest an "early" transition state for reductive elimination by these Ni complexes.

Table 4.2. Reductive Elimination Transition State Geometries[a]

E	NiE	Bite Angle	NiEH	E-C	Ni-C	Ni-P_1	Ni-P_2
CH_2	2.13	91.1	92.5	1.52	2.13	2.17	2.17
NH	1.88	91.3	113.0	1.48	2.23	2.19	2.17
PH	2.16	91.6	111.0	1.88	2.19	2.21	2.18

[a] Bond lengths in Angstrom units; bond angles in degrees

4.3.6 Reductive Elimination Products

The reductive elimination transition state is followed by a product that is an adduct of the three-membered organic ring and the formally zero-valent (dhpe)Ni. For E = NH and PH, coordination through a lone pair on the heteroatom was observed. For E = CH_2, ligation occurred in the plane of one of the strained σ_{CC} bonds of cyclopropane, Figure 4.7.

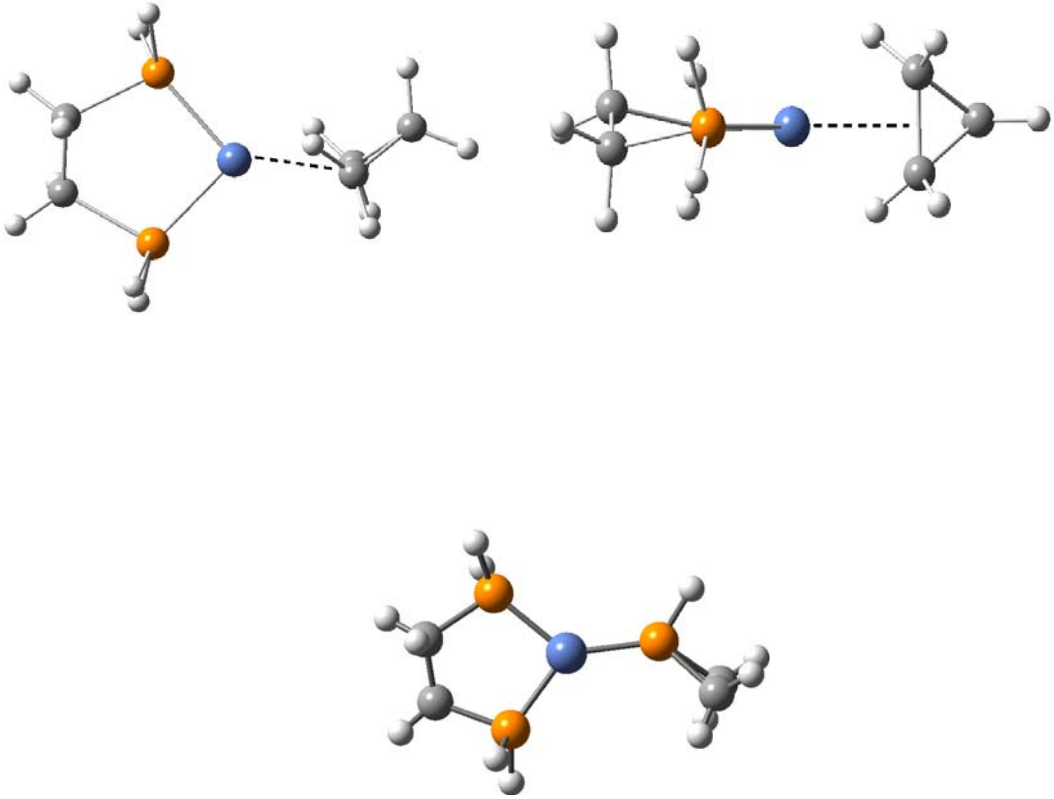

Figure 4.7. Product of reductive elimination of cyclopropane (top) and phosphirane (bottom).

4.3.7 Final Products

The adduct between the three-membered ring product and Ni(dhpe) will undergo dissociation at the expense of another equivalent of ethylene to give the final characterized products of the Hillhouse systems, *i.e.*, (dhpe)Ni(η^2-ethylene) and

corresponding cyclic organic products: cyclopropane, aziridine or phosphirane. Comparison of calculated metric data for the (dhpe)Ni(η^2-ethylene) product showed good agreement with experimental models: Ni-C = 1.98 Å (1.95 – 1.98 Å, expt); Ni-P = 2.17 Å (2.15 – 2.16 Å, expt.); CC = 1.43 Å (1.42 – 1.44 Å, expt.); *bis*-phosphine bite angle = 90° (92°, expt.).[65]

4.4 Energetics

The calculated enthalpic quantities of interest are the barrier to [2+2] addition ($\Delta H^{\ddagger}_{[2+2]}$; π-adduct $\rightarrow$ [2+2] TS), the barrier to reductive elimination ($\Delta H^{\ddagger}_{RE}$; [2+2] intermediate to reductive elimination TS), their corresponding reaction enthalpies ($\Delta H_{[2+2]}$ and ΔH_{RE}), and the overall enthalpy of reaction (ΔH_{rxn}), Table 4.3.

To analyze the thermodynamics, the reaction mechanism is divided into two steps. For the initial step of the reaction sequence ([2+2] addition of ((dhpe)Ni=E to ethylene to yield a 4-membered ring) all the calculated enthalpies ($\Delta H_{[2+2]}$) are very exothermic with the phosphinidene reaction being the least exothermic (-33 kcal/mol) versus the nitrene (-42 kcal/mol) and carbene (-39 kcal/mol) reactions, Table 4.3. For the second step of the reaction (conversion of the [2+2] product to three-membered ring product plus (dhpe)Ni(η^2-ethylene)), reaction enthalpies (ΔH_{RE}) are exothermic with carbene being more exothermic by ~ 12 kcal/mol than the phosphinidene and nitrene transfer, which are of similar exothermicity, Table 4.3. The greater exothermic nature for the formation of the first versus the second E-C bond is reasonable as the [2_π+2_π] process involves transformation of two π-bonds to two σ-bonds in the metallaheterobutane intermediate. As a result of the exothermic nature of the [2_π+2_π]]

step, the overall group transfer is highly exothermic with carbene transfer being the most energetically downhill (ΔH_{rxn} = -57 kcal/mol) and phosphinidene transfer being the least exothermic (ΔH_{rxn} = -39 kcal/mol) and nitrene transfer roughly halfway between these extremes.

Table 4.3. Calculated Enthalpies for Group Transfer (kcal/mol).

E	$\Delta H_{[2+2]}$[a]	ΔH_{RE}[b]	ΔH_{rxn}[c]	$\Delta H^{\ddagger}_{[2+2]}$[d]	$\Delta H^{\ddagger}_{RE}$[e]
CH_2	-39	-18	-57	3	17
NH	-42	-7	-49	4	26
PH	-33	-6	-39	2	12

[a] Enthalpy of formation of metallaheterobutane from separated reactants.
[b] Enthalpy of formation of final products ((dhpe)Ni(η^2-ethylene) + cyclo-EC_2H_4) from metallaheterobutane.
[c] Total reaction enthalpy, *i.e.*, $\underline{\Delta}H_{[2+2]} + \underline{\Delta}H_{RE}$
[d] Enthalpic barrier from π-adduct to [2+2] transition state.
[e] Enthalpic barrier from metallaheterobutane to the reductive elimination transition state.

The enthalpic barrier from the π-adduct to [2+2] transition state ($\Delta H^{\ddagger}_{[2+2]}$) is calculated in the order PH < CH_2 < NH, although the barriers are very small (*i.e.*, ≤ 4 kcal/mol), Table 4.3. A comparison of the reductive elimination barriers ([2+2] intermediate to reductive elimination transition state) yields the following order for $\Delta H^{\ddagger}_{RE}$: PH < CH_2 < NH. The calculated $\Delta H^{\ddagger}_{RE}$ for nitrene transfer displays a considerably higher activation barrier as compared to the corresponding TSs for the carbene and phosphinidene congeners. This result is interesting in light of experimental observations by Hillhouse *et al.*[66] whereby only in the case of nitrogen is a four-membered ring product stable enough to be isolated, albeit for bipyridine and not *bis*-phosphine supporting ligation.

The calculated enthalpic barriers for reductive elimination are ~10 – 20 kcal/mol higher than the corresponding $[2_\pi+2_\pi]$ barriers depending on the group being transferred, Table 4.3. This kinetic discrimination between the two steps of the group transfer mechanism correlates with the thermodynamics calculated for each process. The [2+2] addition to form the first C-E bond is highly exothermic and entails a small kinetic barrier. The reductive elimination to form the second C-E bond is much less exothermic and thus involves a larger barrier. Hence, the present calculations suggest that the rate-determining step for nickel-mediated group transfer to ethylene is reductive elimination from the metallaheterobutane.

To support the observed results and to obtain more information on the relative stabilities of Ni=E complexes, a series of calculations are carried out to estimate the relative Ni=E, Ni-E, C-E and E-E bond enthalpies. The following reactions are used to determine the required enthalpies.

$$2\ (dhpe)Ni + E{=}E \dashrightarrow 2\ (dhpe)Ni{=}E \qquad (4.2)$$

$$2\ (dhpe)Ni + H\ E\text{-}E\ H \dashrightarrow 2\ (dhpe)Ni(\text{-}EH)_2 \qquad (4.3)$$

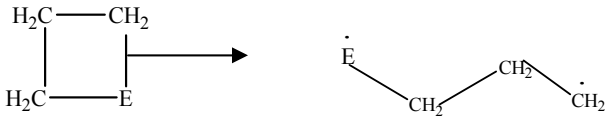

(4.4)

The bond enthalpies of Ni=E, E=E and E-C are defined using the following equations.

$$BE_{Ni=E} \equiv (BE_{E=E} - \Delta H_1) \div 2 \qquad (4.5)$$
$$BE_{Ni-E} \equiv (BE_{E-E} - \Delta H_2) \div 2 \qquad (4.6)$$
$$\pi_{Ni-E} \equiv BE_{Ni=E} - BE_{Ni-E} \qquad (4.7)$$
$$\pi_{E-E} \equiv BE_{E=E} - BE_{E-E} \qquad (4.8)$$
$$\Delta_{E-C} \equiv \Delta H_3 \qquad (4.9)$$

The quantities ΔH_1 and ΔH_2 represents the reaction enthalpies for different E (CH_2, NH, PH) of equations 1 and 2, respectively. The bond dissociation enthalpies for E=E and E-E are determined from the reaction enthalpies for homolytic dissociation of E=E and E-E. $BE_{Ni=E}$ corresponds to the (σ + π) bond enthalpy whereas BE_{Ni-E} corresponds to the σ-bond enthalpy only. The calculated Δ_{Ni-E}, Δ_{Ni-E}, Δ_{E-E} and σ_{C-E} bond enthalpies are shown in Table 4.4.

Table 4.4. Estimated Bond Enthalpies (kcal/mol)

E	σ_{Ni-E}	π_{Ni-E}	π_{E-E}	σ_{E-C}
CH_2	41	29	77	55
NH	49	7	51	49
PH	41	12	21	43

Since the second step (reductive elimination step) of the putative mechanism is the rate determining step, a comparison has been made between the estimated bond enthalpies from Table 4.4 and the calculated activation barrier enthalpies and reaction enthalpies. The reductive elimination step (conversion of the [2+2] product to final products) is characterized by two bond enthalpies: breaking of a σ_{Ni-E} bond, and making of a σ_{E-C} bond. Since the reductive elimination transition state is relatively early, its geometry will be close to its precursor [2+2] product. Hence one would expect, and indeed obtains good correlations between the σ_{Ni-E} bond enthalpies and the activation barrier enthalpies as well as the reaction enthalpies and σ_{E-C} bond enthalpies.

4.5 Conclusions

Density functional theory is used to determine the thermodynamic (ground state) and kinetic (transition state) feasibility of Ni=E (E = CH_2, NH, PH) mediated group transfer (E) to ethylene to form three-membered ring products. Nickel complexes

chosen for this research are models of recent complexes reported by Hillhouse and coworkers. Based on DFT geometry optimizations it is concluded that the (dhpe)Ni=O congener would be unstable, rearranging to a phosphine oxide. From the calculated enthalpies of the individual reaction steps, as well as the enthalpic barriers, (dhpe)Ni system is a potent system for heterogroup transfer to olefins to synthesize cyclic organics, *i.e.*, aziridines, cyclopropanes and phosphoranes.

The individual steps and overall reaction are highly exothermic for all transfer groups investigated: nitrene, carbene and phosphinidene. The order of increasing exothermicity for Ni-mediated group transfer is PH < NH < CH_2.

All [2+2] transition states are accompanied by the dissociation of one of the Ni-P bonds of dhpe in the transition state. When the [2+2] intermediates are subsequently formed, the *bis*-phosphine reverts to η^2 coordination. Thus, a change in hapticity of the dhpe ligand from $\eta^2 \rightarrow \eta^1 \rightarrow \eta^2$ is calculated along the [2+2] reaction pathway.[67]

Calculations indicate that reductive elimination from the four-membered metallaheterobutane intermediate is the rate-determining step of the mechanism for all E. The greater kinetic barrier to reductive elimination relative to $[2_\pi+2_\pi]$ addition is consistent with the lower thermodynamic driving force for the former.

CHAPTER 5

ROLE OF SPIN STATE AND COORDINATION NUMBER ON C-H ACTIVATION BY FE-IMIDO COMPLEXES

5.1 Introduction

Three-coordinate complexes of the transition metals remain relatively rare although recent synthetic efforts have yielded new examples with interesting chemistry.[68] It is expected that their electronic and steric unsaturation can be crucial in organometallic catalysis. Holland and coworkers have extensively investigated the bonding, structure and reactivity of novel three-coordinate species with β-diketiminate supporting ligation, both as stable isolable entities as well as metastable reaction intermediates.[69] The β–diketiminate ligand functions as a monoanionic bidentate ligand, which has been applied to the synthesis of a wide variety of transition metal, main group element, and lanthanide complexes.[70] These ligands display strong binding to metals, and flexible stereoelectronic demands as observed, for example, in the reversible β-hydrogen elimination of Fe(β-diketiminate)-alkyl complexes and in the reactions of Fe(β-diketiminate) complexes with dinitrogen.[69]

Amido (L_nM-NR_2) complexes of the late transition metals have also received increased attention,[71] primarily because of their participation in important catalytic processes such as amination[72] and carbon-hydrogen bond activation.[73] Holland *et al.*[74] have reported iron-amido complexes of the type L^RFe^{II}-N(H)Ar where L = β-diketiminate; R = methyl, *tert*-butyl; Ar = *para*-tolyl, 2,6-xylyl, which are high spin (quintet) complexes that undergo protonation by terminal alkynes and alcohols to give free H_2NAr and three coordinate acetylide and alkoxide complexes, respectively.

The synthesis and reactivity of transition metal imido/nitrene ($L_nM=NR$) complexes has also been an area of considerable interest over the last twenty years.[73a] However, terminal imido complexes of the later transition metals (group 8 and beyond) remain relatively rare, a situation typically ascribed to the lack of empty dπ orbitals suitable for stabilization of the lone pairs of the NR^{2-}moiety.[75] Studies on imido complexes of group 8 - 10 metals[76] have focused on imido group transfer, [74b,f,k] and the activation of H_2.[74c,e]

It has been proposed that multiply bonded transition metal complexes may be formed in the reduction of dinitrogen.[69b,c] The active sites in the industrial Haber-Bosch and biological nitrogenase catalysts contain iron, as a result, studying terminal Fe=NR species is therefore of considerable interest. Mononuclear iron-imido complexes have been reported by Peters[77] and coworkers, *viz* $[PhB(CH_2PPh_2)_3]Fe{\equiv}NR$, which are characterized by a strong, formally iron nitrogen triple bond. The Fe^{III}-imido complexes synthesized by Peters *et al.* possess a low spin (doublet) ground state and undergo reactions with dihydrogen under ambient conditions. These initial studies lead Holland *et al.* to study carbon-hydrogen bond activation by transient $L^RFe=NAd$ (Ad = 1-adamantyl) complexes.[78]

Although terminal iron-imido complexes have not been directly observed until recently, the study of their reactions is given extra impetus as they can be considered analogues of Fe-oxo (ferryl) complexes, the putative active oxidant in cytochrome P-450.[79] Theoretical calculations by Yoshizawa[80] on C-H bond activation of alkanes by iron-oxo complexes proposed a direct abstraction method with a linear C···H···O···Fe

transition state. An analysis of C-H activation by FeO^+ by Shaik *et al.*, led to the proposal of a two-state reactivity (TSR) model.[81]

The goal of this research is to assess the role of iron coordination number and spin state in carbon-hydrogen bond activation by Fe(β-diketiminate)-imido complexes. Preliminary calculations have been performed at the DFT level on smaller computational models and then extended to full experimental models.

5.2 Computational Methods

The Gaussian[30](98 and 03) packages were used for this research unless noted otherwise. The B3LYP hybrid functional was employed.[23,25] For iron and all main group elements the effective core potential (ECP)[27] and valence basis sets of Stephens, Basch and Krauss (CEP-31G) was employed,[28] augmented with a d-polarization function for main group elements (with corresponding exponent of 0.8 for carbon and nitrogen). The Stevens ECP basis sets are valence triple zeta for transition metals and double zeta for main group elements. The –31G basis set was employed for hydrogen.

Hybrid quantum mechanics/molecular mechanics (QM/MM) calculations were used to study full experimental models of the proposed imido intermediates: $L^{Me}Fe{=}NAd$ and $L^{Me}Fe(4^tBuPy)(=NAd)$. The QM/MM calculations utilized the ONIOM[26] methodology within the Gaussian suite of programs. The B3LYP/6-31G(d) level of theory was applied to the QM region; the MM region included the bulky substituents (Ar and Me substituents of L^{Me} and the entire adamantyl group except the carbon directly attached to the imido nitrogen). The MM interactions were modeled with the Universal force field (UFF).[82]

Reactant, transition state and product geometries were fully optimized using gradient methods. The unrestricted Kohn-Sham formalism was used for the description of all open-shell species, unless otherwise noted. The energy Hessian was calculated and thus confirmed the stationary points as minima (no imaginary frequencies) or transition states (one imaginary frequency). All reported enthalpies are calculated at 1 atm and 298.15K.

5.3 Results and Discussions

The base molecules used for modeling purposes of a three- and four-coordinate iron-imido complex are L'Fe=NH and L'Fe(NH_3)(=NH), respectively. The simplest β-diketiminate model L' ($C_3N_2H_5^-$) is employed. This approximation has been used before in previous studies of Fe(β-diketiminate) complexes and shown to faithfully reproduce the electronic and energetic profile of the full experimental ligand system.[69]

The model complexes L'Fe(=NH) and L'Fe(=NH)(NH_3) were investigated in the low (multiplicity = 2), intermediate (mulitiplicity = 4), and high-spin (multiplicity = 6) states permissible to an iron complex with a formal oxidation state of +3 (*i.e.*, d^5), Scheme 5.1.

The density functional calculations were complicated by spin contamination, particularly for the IS and LS states, due to the unrestricted Kohn-Sham formalism employed (restricted open-shell DFT formalisms did not yield SCF convergence). With this caveat in mind the results of the DFT calculations imply that there is a dense manifold of low energy states of differing multiplicity. For the three-coordinate imido models, the enthalpic ordering is IS < HS << LS. For the four-coordinate imido model,

the calculated enthalpies of different multiplicity states showed the order IS ~ HS << LS. Since for both 3- and 4- coordination Fe-imide complexes, the low spin (doublet) states are very high in enthalpy as compared to intermediate spin (quartet) and high spin (sextet) states, we neglected the doublet spin state in the remainder of the calculations.

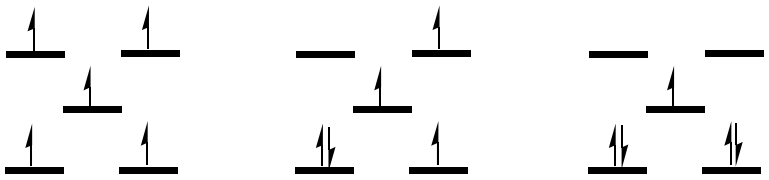

high spin (HS) | intermediate spin (IS) | low spin (LS)

Scheme 5.1

5.3.1 Three- and Four-Coordinate Imido Geometries

Geometry optimization of the imido complexes (spin states of 2, 4, 6) at the B3LYP/CEP-31G (d) level of theory leads to several minima. The calculated energetics at this level of theory indicate that L'Fe=NH is most stable at the intermediate (quartet) spin state, being 10 kcal/mol below the doublet and 15 kcal/mol more stable than the sextet. For the four-coordinate model, L'Fe(NH_3)(=NH), IS and HS states are closer energetically: IS < HS (4 kcal/mol) < LS (8 kcal/mol). The iron coordination geometries for the three-coordinate imido models are all trigonal planar, regardless of spin state. The expected trend of increasing metal-ligand bond lengths with higher multiplicities is seen, Table 5.1. For the four-coordinate imido models (Table 5.1 and Figure 5.1) the high, intermediate and low spin complexes are tetrahedral, trigonal-monopyramidal, and square planar, respectively.

Table 5.1: Calculated Geometries for Truncated Imido Models[a]

	HS	IS	LS
L' Fe=NH			
Fe=N	1.94	1.76	1.67
Fe-N_1	2.01	1.97	1.90
Fe-N_2	2.00	1.97	1.90
N_1Fe=N	122.2	133.1	134.6
N_2Fe=N	143.3	133.2	134.6
N_1FeN_2	94.5	93.3	90.1
Fe=NH	125.0	136.8	180.0
L'Fe(NH_3)(=NH)			
Fe=N	1.76	1.83	1.82
Fe-NH_3	2.22	2.26	2.09
Fe-N_1	2.05	2.01	1.95
Fe-N_2	2.04	2.00	1.90
H_3NFeN_1	101.5	99.9	91.3
H_3NFeN_2	105.3	100.3	178.0
H_3NFe-N	99.6	91.3	82.6
N_1Fe=N	115.7	132.4	174.0
N_2Fe=N	137.6	131.1	95.4
N_2FeN_1	92.3	92.3	90.7
Fe=NH	152.7	124.2	118.2

[a]Bond lengths in Angstrom units; bond angles in degrees. Geometries determined at the B3LYP/CEP-31G(d) level of theory. N_1 and N_2 in Table 5.1 denote β-diketiminate nitrogens.

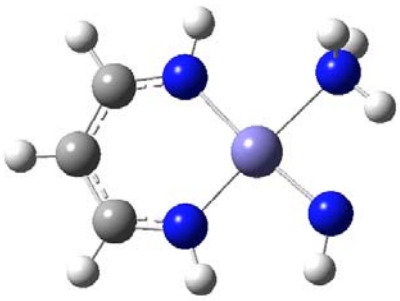

Doublet

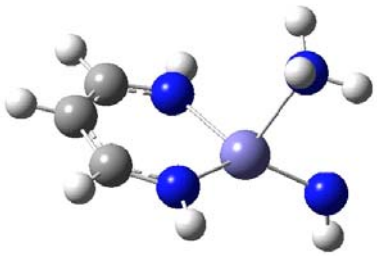

Quartet

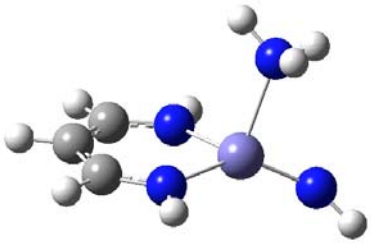

Sextet

Figure 5.1 Geometries of four coordinated imido complexes.

5.3.2 Full Experimental Imido Complexes

After preliminary investigation of the small imido models, the calculations were extended to the full models proposed (but not isolated and structurally characterized) by Holland *et al.*,[78] $L^{Me}Fe{=}NAd$ and $L^{Me}Fe(4^{t}BuPy)(=NAd)$, Figure 5.2. Although the isolation of three and four-coordinated Fe-imido complexes was not possible, the combination of spectroscopic results including NMR (Fourier-transform infrared) and EPR (electron paramagnetic resonance) and Mossbauer spectroscopy suggested that the three-coordinate iron(III) imido complex, $L^{Me}Fe{=}NAd$ is in rapid equilibrium with $L^{Me}Fe(4^{t}BuPy)(=NAd)$.[78] The low energy sextet and quartet spin states were the focus of this computational investigation.

Enthalpy comparisons indicate that the Fe^{III}-imido complex $L^{Me}Fe{=}NAd$ is more stable as a quartet, Figure 5.2 (top), by 9 kcal/mol versus the sextet. The calculated ground state thus mirrors that for the DFT calculations on L'Fe=NH. However, in the case of $L^{Me}Fe(4^{t}BuPy)(=NAd)$ the sextet state is now more stable by 2 kcal/mol than the quartet, Figure 5.2 (bottom). Geometry optimization of $L^{Me}Fe{=}NAd$ yielded a trigonal planar coordination geometry for iron for both spin states whereas optimization of high spin $L^{Me}Fe(4^{t}BuPy)(=NAd)$ yielded a tetrahedral coordination geometry; the quartet spin state has a trigonal monopyramidal iron coordination environment, Table 5.2. The tetrahedral geometry of high spin $L^{Me}Fe(4^{t}BuPy)(=NAd)$ is consistent with its d^5 electronic configuration, and is supported by crystal structures on Fe^{III} complexes of the type $L^{R}FeX_2$.[83]

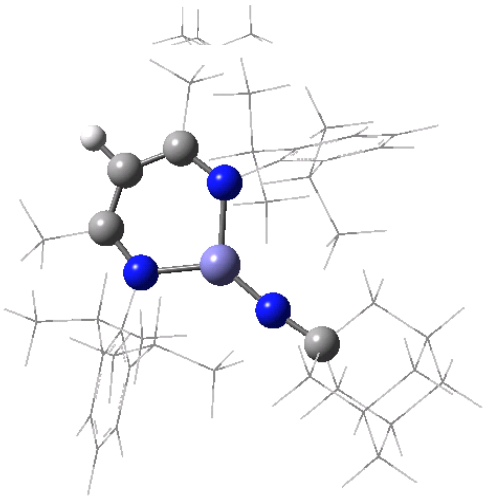

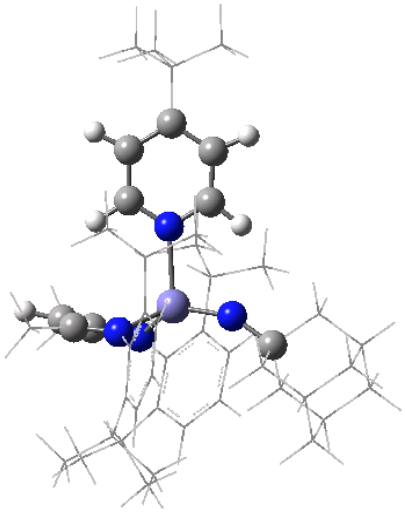

Figure 5.2: QM/MM-optimized geometries of quartet $L^{Me}Fe{=}NAd$ (top) and sextet $L^{Me}Fe(4^{t}BuPy)(=NAd)$ (bottom). MM atoms are shown in wireframe, the remainder is modeled with QM (B3LYP/6-31G (d)) methods. The universival force field is employed for molecular mechanics region.

Table 5.2. QM/MM Optimized Geometries for $L^{Me}Fe{=}NAd$ & $^{Me}Fe(4^{t}BuPy)(=NAd)^{a}$

	HS	IS
$L^{Me}Fe{=}NAd$		
Fe=N	1.71	1.67 Å
Fe-N_1	1.97	1.89 Å
Fe-N_2	2.03	1.90 Å
N_1FeN	154.5	135.6º
N_2FeN	109.8	127.6º
N_1FeN_2	93.1	96.9º
$FeNC_{Ad}$	167.1	174.0º
$L^{Me}Fe(4tBuPy)(=NAd)$		
Fe=N	1.74	1.75
Fe-N_{py}	2.18	2.20
Fe-N_1	2.05	1.98
Fe-N_2	2.06	1.99
$N_{py}FeN_1$	110.1	98.4
$N_{py}FeN_2$	109.0	98.2
$N_{py}FeN$	102.6	99.2
N_1FeN	116.2	122.7
N_2FeN	127.8	130.9
N_2FeN_1	90.3	99.4
$FeNC_{Ad}$	155.1	152.0

[a]Bond lengths in Angstrom units; bond angles in degrees. Geometries determined at ONIOM(B3LYP/6-31G(d):UFF) level of theory for high spin (HS, sextet), and intermediate spin (IS, quartet). N_1 and N_2 denote β-diketiminate nitrogens.

5.3.3 Electronic Structure of Full Imido Complexes

Full quantum calculations on full imido models were not successful in our hands with the Gaussian program due to SCF convergence failure. Hence, single-point calculations with a comparable quantum treatment (ROB3LYP/CSDZ*) were performed with the Jaguar parallel quantum chemistry program[84] at the ONIOM-optimized minima of $L^{Me}Fe(4^tBuPy)(=NAd)$ and $L^{Me}Fe=NAd$ to give insight into (a) the d-orbital splitting of the d^5-Fe^{III} ion, (b) the nature of $Fe=N_{imido}$ π-bond in these imido complexes, and (c) the unexpected shift in ground state from IS to HS upon coordination of a fourth ligand to the imido. A restricted open-shell Kohn-Sham formalism was utilized to ease frontier orbital analysis, and preclude spin contamination effects. As the quartet states entail unequal occupation numbers for the d orbitals of Fe^{III}, the extended Hückel semiempirical method (HyperChem program[85]) was used to provide a qualitative estimate of the relative d orbital energies for these complexes. The orbital splitting and orbital compositions among all methods employed closely mirror each other. Figure 5.3 depicts the frontier Kohn-Sham orbitals of the full three- and four- coordinate imido complexes at their ONIOM[26]-determined ground states of quartet and sextet, respectively. Both the three-coordinate and the four-coordinate complexes show Fe-N π character (d_{yz} and d_{xz}), supporting the argument that the Fe-N_{imido} linkage has substantial multiple bond character.

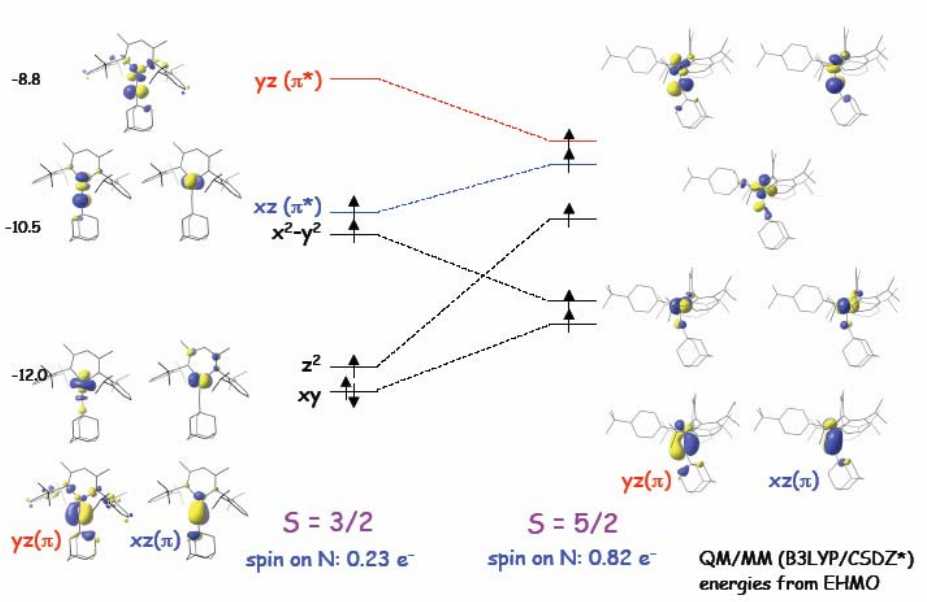

Figure 5.3: Qualitative MO correlation diagram for quartet $L^{Me}Fe{=}NAd$ (left) and sextet $L^{Me}Fe(4^{t}BuPy)(=NAd)$.

In the quartet three-coordinate imido (left hand side of Figure 5.3) the FeN_{imido} $\pi^*(yz)$ orbital is unoccupied, and higher in energy than the corresponding $\pi^*(xz)$ because of antibonding interactions with the diketiminate nitrogen atoms. For the high-spin, four-coordinate imido complex, both Fe-N_{imido} π^* orbitals are, of course, equally occupied by one electron. Thus, this implies a rough FeN_{imido} bond order (assuming the σ bond order is 1) of 2.5 for IS-$L^{Me}Fe{=}NAd$, and 2.0 for HS-$L^{Me}Fe(4^{t}BuPy)(=NAd)$. Furthermore, this qualitative picture also supports more significant spin density on the imido nitrogen, particularly given the covalent nature of these π^* orbitals. The QM/MM calculations further support the spin density arguments; as we move from IS-$L^{Me}Fe{=}NAd$ to HS-$L^{Me}Fe(4^{t}BuPy)(=NAd)$ the calculated spin density on the imido nitrogen more than triples from 0.23 to 0.82 e^-.

We now turn our attention to the counterintuitive change to a higher spin state upon coordination of $4^{t}BuPy$. *A priori*, one expects that coordination of an extra ligand

to a transition metal to increase the d-orbital splitting, pushing the energetic balance away from higher spin states towards lower spin states. However, it must be remembered that the coordination of 4^{t}BuPy also entails a geometrical distortion of the L^{Me}Fe=NAd moiety from trigonal planar to pyramidal. To enumerate the effect of pyramidal distortion on spin state preferences, a simple calculational "experiment" was performed.

The quartet and sextet states of a hypothetical pyramidal L^{Me}Fe=NAd (generated by deletion of 4^{t}BuPy from the QM/MM-optimized geometry of HS-L^{Me}Fe(4^{t}BuPy)(=NAd) without geometric relaxation) were studied at the ONIOM(B3LYP/6-31G(d):UFF) level of theory. Unlike the fully optimized (and thus trigonal planar) L^{Me}Fe=NAd, the pyramidal geometry shows a shift to a sextet ground state (by 1.5 kcal/mol). Hence, assuming that coordination of 4^{t}BuPy to Fe^{III} has the expected effect to increase d orbital splitting, calculations suggest that this is more than countermanded by the pyramidalization of the L^{Me}Fe=NAd core that takes place upon formation of the four-coordinate imido. Taken together, the electronic structure analysis implies an enhancement of the radical reactivity upon ligation of a fourth ligand, and the accompanying change in spin state from quartet to sextet. These observations support the arguments derived from experiments, *i.e.,* that it is the four-coordinate Fe^{III}-imido complexes that are the active species in the system studied by Holland *et al.*[78]

5.3.4 Amido Product Geometries

Calculations were extended to full experimental models of Fe^{II}-amido complexes, which are the products of hydrogen atom abstraction (HAA) of hydrocarbons by Fe^{III}-imido complexes proposed- L^{Me}Fe-N(H)Ad and L^{Me}Fe(4^{t}BuPy)(N(H)Ad), at both triplet and quintet spin states.[78] Geometry optimizations of amido complexes used the same QM/MM partitioning scheme applied to the full imido models. The QM/MM calculations indicated that the quintet amido product is more stable than the triplet amido by 12 kcal/mol for L^{Me}Fe-N(H)Ad and 18 kcal/mol for L^{Me}Fe(4^{t}BuPy)(-N(H)Ad), consistent with experimental magnetic moments, which point to a quintet ground state for Fe^{II}-amido complexes with β-diketiminate supporting ligation.[78] Thus, irrespective of the spin state for both three and four coordinated Fe-imido reactants, a stable quintet amido product is predicted computationally and observed experimentally.

The geometries of L^{R}Fe-N(H)R' are quite sensitive to the particular amido (R') and β-diketiminate (R) substituent, as well as the presence or absence of a fourth ligand, but a comparison of QM/MM-calculated bond lengths and angles shows good agreement with experimental averages. Note that for the full amido models there is an asymmetry in the N_b-Fe-N_{amido} angles, large Fe-N_{amido}-C_{Ad} angles (~136 - 138°), and corresponding small Fe-N_{amido}-H_{amido} angles (~113°). These yield Fe...H_{amido} distances of ~2.5 Å, suggestive of a weak agostic interaction involving the amido hydrogen.

Table 5.3. Experimental and Calculated Geometries of Fe(β-diketiminate) Amido Complexes[a, 78]

	Experiment		Computation	
	Three-Coord.	Four-Coord.	Three-Coord.	Four-Coord.
Fe-N_{amido}	1.88(5)	1.93(5)	1.85	1.91
FeN_{β}	1.99(2)	2.03(1)	1.96	2.02
			1.97	2.01
$N_{\beta}FeN'_{\beta}$	94.3(4)	95.1(8)	95.9	95.6
$N_{\beta}FeN_{amido}$	133(18)	121(18)	145.4	134.5
$N_{\beta}FeN$	--	--	--	99.6

[a] Computed values: bond length is in Å and bond angle is in °

The optimization of full models of the imidos and amidos requires only the calculated enthalpy of H• to estimate N_{amido}-H homolytic bond dissociation enthalpies. For the three-coordinate amido (quintet ground state), the N_{amido}-H_{amido} bond enthalpy is calculated to be 80 kcal/mol relative to the calculated quartet ground state of L^{Me}Fe=NAd. The four-coordinate amido, has a N-H bond enthalpy of 73 kcal/mol, calculated relative to the sextet ground state of L^{Me}Fe(4^{t}BuPy)(=NAd). As a reference, ONIOM(B3LYP/6-31G(d):UFF) calculations using the same QM/MM partition as in the iron complexes yield a BDE of 81 kcal/mol for ^{2}N(H)Ad → ^{3}NAd + ^{2}H. These values are significantly less than the parent species (triplet-HN + doublet-H• → doublet-H_2N•, ΔH_{calc} = -89 kcal/mol, obtained by the highly accurate G3[86] method; -92 kcal/mol using the DFT methods employed in this research).

The calculated N-H bond dissociation enthalpies for the full Fe^{II}-amido/Fe^{III}-imido models are, consistent with the putative imido species characterized, which is able to only activate weak C-H bonds such as those in 1,4-cyclohexadiene, which has an estimated homolytic bond enthalpy of 75(2) kcal mol for the double allylic C-H bond.[77] Full QM calculations (B3LYP/CEP-31G(d)) yield a C-H bond energy of 72 kcal/mol for 1,4-cyclohexadiene.

5.3.5 Transition States

Transition states for the C-H activation of methane (truncated models) and 1,4-cyclohexadience (full models) were isolated with DFT and hybrid DFT/MM methods, respectively, for both IS and HS states. We focus our attention on the latter as these are better models of the systems of greatest experimental interest.

Figure 5.7 depicts the transition state for C-H activation of the *bis*-allylic C-H bonds of 1,4-cyclohexadiene by sextet- $L^{Me}Fe(4^{t}BuPy)(=NAd)$. The active site involves a linear three-center N_{imido}•••H•••C with N_{imido}•••H = (1.35 Å for three-coordinate quartet, 1.42 Å for three-coordinate sextet; 1.37 Å for four-coordinate quartet and 1.37 Å for four-coordinate sextet,) and C•••H = (1.31 Å for three-coordinate quartet, 1.27 Å for three-coordinate sextet; 1.32 Å for four-coordinate quartet and 1.35 Å for four-coordinate sextet). The other transition states are similar in structure regardless of spin state or iron coordination number.

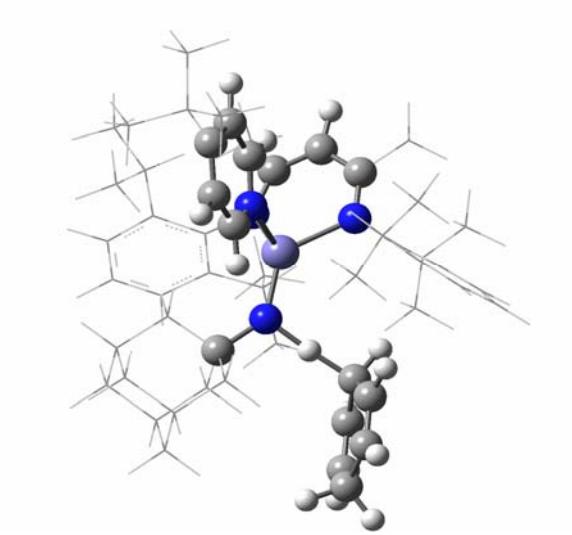

Figure 5.4: QM/MM-calculated transition state for C-H activation of 1,4-cyclohexadiene by quartet $L^{Me}Fe(4^{t}BuPy)$.MM atoms shown in wireframe, remainder calculated using QM methods.

The calculated three-coordinate transition state, Figure 5.4, places the CHD substrate on the opposite side of the equatorial plane (defined by the β-diketiminate and imido nitrogens) away from the $4^{t}BuPy$ donor ligand. The following cartoon (Scheme 5.2) shows the above described 1,4cycloheaxadiene C-H activation.

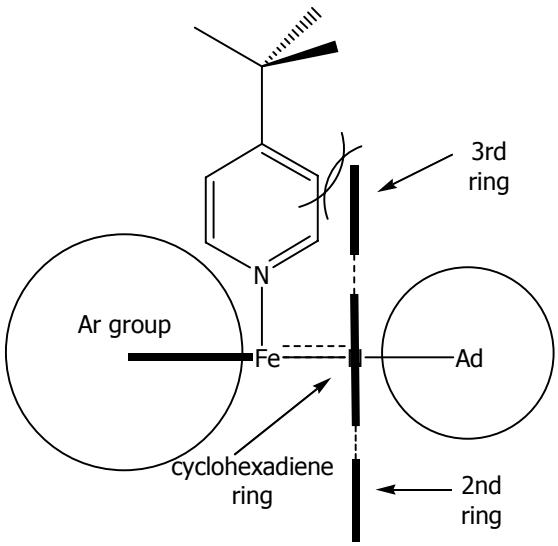

Scheme 5.2

As such, the position of the 1,4-cyclohexadienyl group is sterically constrained by the adamantyl substituent of the imido ligand and one of the 2,6-$C_6H_3iPr_2$ substituents of the β-diketiminate ligand. Molecular mechanics calculations using the QM/MM-optimized transition states as a fixed scaffold and modifying the substrate orientation (replace cyclohexadienyl with both indenyl and 9,10-dihydroanhtracenyl substituents) indicates that while there is sufficient room to dock an indene substrate to the Fe-imido active site, the docking of a three-ring substrate like 9,10-dihydroanthracene is sterically hindered. Furthermore, the MM calculations indicate that while the steric impediment for DHA (versus CD) is minimal for a three coordinate TS model, it is more pronounced for a four-coordinate TS model. These MM results are consistent with the experimentally observed selectivity patterns (indene and CD are activated, but DHA is not)[78] and further supports the proposed transition state models vis-à-vis metal coordination number for the active imido species.

5.3.6 Full Experimental Model Reaction Enthalpies

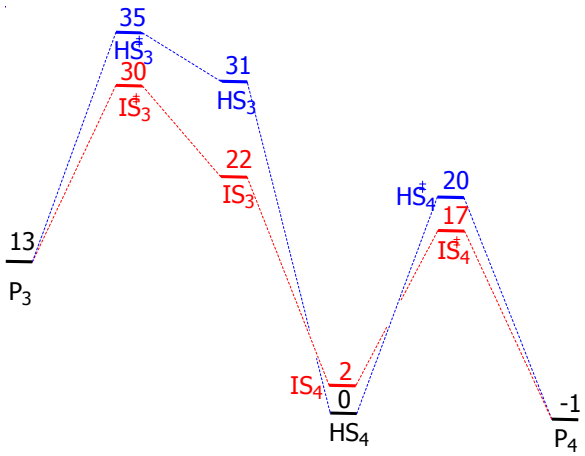

Figure 5.5: Reaction coordinate for activation of 1,4-cyclohexadiene by $L^{Me}Fe(4^tBuPy)(=NAd)$ and $L^{Me}Fe=NAd$. Calculated enthalpies are denoted in kcal/mol, and are relative to HS_4. P_3 = quintet-$L^{Me}Fe$-N(H)Ad + 1,4-cyclohexadienyl radical; $HS^{\ddagger}_3$ and $IS^{\ddagger}_3$ = transition state for C-H activation of 1,4-cyclohexadiene by sextet- and quartet-

$L^{Me}Fe$=NAd, respectively; HS_3 and IS_3 = sextet- and quartet-$L^{Me}Fe$=NAd, respectively; HS_4 and IS_4 = sextet- and quartet- $L^{Me}Fe(4^tBuPy)$(=NAd), respectively; $HS^{\ddagger}_4$ and $IS^{\ddagger}_4$ = transition state for C-H activation of 1,4-cyclohexadiene by sextet- and quartet-$L^{Me}Fe(4^tBuPy)$(=NAd), respectively; P_4 = quintet-$L^{Me}Fe(4^tBuPy)$(N(H)Ad) + 1,4-cyclohexadienyl radical.

Shown in Figure 5.5 is a reaction coordinate depicting enthalpy for the various important stationary points for the full QM/MM models - intermediate and high spin imido (three- and four-coordinate variants) and 1,4-cyclohexadiene reactants, transition states and quintet amido and 1,4-cyclohexadienyl radical products. Overall, the most thermodynamically stable ground states are the quartet- and sextet-$L^{Me}Fe(4^tBuPy)$(=NAd) species, with the intermediate spin (quartet) state calculated to be 2 kcal/mol below the corresponding high spin (sextet) state. Given the level of theory employed, it is not possible to state with complete certainty which of these spin states is the ground state, but one can easily conclude that the two spin states are indeed energetically competitive in the four-coordinate imido, while for the three-coordinate imidos the quartet is clearly the ground state, an inference consistent with ESR and Mossbauer spectroscopy[77] (Mossbauer calculations are discussed in section 5.5).

The ground state stability for the four-coordinate imido reactants versus three-coordinate analogues (due to the stability of coordination of 4-tert-butyl-pyridine) is manifested in the stability of their C-H activation transition states. Note that there has been a crossover in the calculated spin state ordering for the four-coordinate imido reactants (sextet < quartet) as compared to the transition states (quartet < sextet). As with the ground state energy differences, the transition state energy differences are

small (3 kcal/mol), likely approaching the limit of discernability for models of this size. Regardless, both of the four-coordinate C-H activation transition states are enthalpically more stable than their three-coordinate congeners by roughly 12 kcal/mol. Hence, the calculations indicate that the major pathway to C-H activation in these Fe^{III}-β-diketiminate-imido complexes passes through a four-coordinate active species.

5.4 NMR Calculations

Due to the lack of the crystal structures for $L^{Me}Fe(=NAd)$ and $L^{Me}Fe(4^{t}BuPy)(=NAd)$, NMR and Mossbauer spectroscopy experiments were performed to support the arguments as to the nature of the proposed imido active species. Using the methods developed by Oldfield *et al.*, for studying the NMR properties of iron complexes,[87] calculations were carried out to predict ^{1}H NMR spectra of $L^{Me}Fe(=NAd)$ and $L^{Me}Fe(4^{t}BuPy)(=NAd)$ for both HS and IS states. The spectra thus obtained were compared with experimental ^{1}H NMR spectra.

Gaussian03[29] was used to determine the ^{1}H NMR chemical shifts for the quartet and sextet states of $L^{Me}FeNAd$ and $L^{Me}Fe(4\text{-t-buPy})NAd$. The NMR calculations (GIAO approximation[88]) were carried out at the QM/MM-optimized geometries for each coordination number and spin state. The B3LYP Hamiltonian was employed, as this level of theory has been shown to give accurate results for the prediction of NMR and Mossbauer spectroscopy for diamagnetic and paramagnetic iron complexes of varying spin states, oxidation states and ligand environments.[89]

To calculate the Fermi contact spin density and isotropic magnetic shielding tensors the following basis sets were used: Wachters' all-electron basis

(62111111/3311111/3111) for Fe, 6-311G* for carbon and nitrogen, and 6-31G* for hydrogen atoms.[90] Oldfield *et al* have extensively used this "locally dense" scheme to enable accurate predictions of these spectroscopic properties. Oldfield *et al*. proposed that a "locally dense" scheme is important in modeling the metal center, which requires a large number of basis functions for accurate description of the quadrupole splitting and hyperfine shifts.

The three-coordinated imido complex L^{Me}FeNAd has 56 hydrogens, and the four coordinated imido complex L^{Me}Fe(4-t-Bu-Py)NAd has 69 hydrogens. Based on their chemical connectivity, the protons in these complexes have been grouped into 8 types for the former and 11 proton types for the latter (Figure 5.6). The observed chemical shift in paramagnetic species can be described as

$$\delta_{obs} = \delta_{dia} + \delta_{hf} \qquad (5.1)$$

where, $\delta_{obs,}$ $\delta_{dia,}$ δ_{hf} are the observed, diamagnetic and paramagnetic (hyperfine) shifts, respectively.

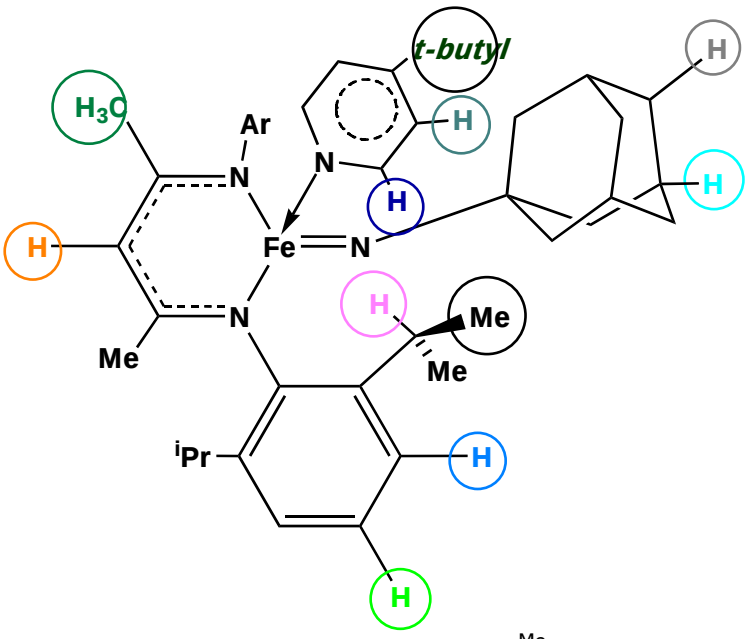

Figure 5.6 Chemically different types of protons in L^{Me}Fe(4-t-Bu-Py)NAd.

An attempt was made to compare the calculated NMR shifts with experimental NMR shifts. Since the experimental NMR shifts for these paramagnetic species are based on relative integration, we focused on those proton assignments deemed most experimentally reliable, *i.e.*, the hydrogens of the β-Me of the β-diketiminate ligand (integrates uniquely to 6 protons) and the para hydrogens on the phenyl ring of 2,6-$C_6H_3{}^iPr_2$ (integrates uniquely to 2 protons). For the β-Me protons it is likely there is torsion about the C-C bond in solution and so these protons would thus be rotationally averaged. However, the 2,6-$C_6H_3{}^iPr_2$ ring is expected to be reasonably static, even in solution, and thus its protons may be considered to be the most reliable.

Table 5.4 show the average calculated proton shifts (ppm) for β-Me hydrogens of the β-diketiminate ligand and the para hydrogens on the phenyl ring of 2,6-$C_6H_3{}^iPr_2$ for all imido spin and coordination states that were studied.

Table 5.4. Calculated ^{1}H NMR Data for IS (quartet) and HS (sextet) of L^{Me}FeNAd and L^{Me}Fe(4-t-Bu-Py)NAd

	β-Methyl-H		Para-H	
	Ave. δ_{obs}	Degeneracy	Ave. δ_{obs}	Degeneracy
L^{Me}FeNAd - IS	-90.8	6	-23.8	2
L^{Me}FeNAd - HS	8.7	1	-41.5	1
	22.4	2	-8.2	1
	28.2	1		
	40.9	1		
	84.5	1		
L^{Me}Fe(4-t-Bu-Py)NAd - IS	-165.8	1	-28.3	2
	-151.4	1		
	-137.0	1		
	-125.7	1		
	-7.1	2		
L^{Me}Fe(4-t-Bu-Py)NAd - HS	-4.3	1	-21.4	1
	-2.0	1	-12.5	1
	44.5	1		
	55.6	1		
	129.0	1		
	157.9	1		

Comparison of the calculated and experimental proton NMR shows much better correlation for quartet complexes than their sextet counterparts. Calculated ^{1}H NMR shifts for the para-hydrogens are –23.8 ppm (2H, L^{Me}FeNAd) and -28.3 ppm (2H, L^{Me}Fe(4-t-Bu-Py)NAd) compared to the experimental assignment[77] of -27 ppm (integration = 2H). However, in the case of sextet complexes, both three- and four-coordinate complexes showed the two para-hydrogens to be split in the ^{1}H NMR spectra: –41.5 ppm and -8.2 ppm (L^{Me}FeNAd); –21.4 ppm and –12.5 ppm (L^{Me}Fe(4-t-Bu-Py)NAd). Thus, calculated NMR chemical shifts showed better agreement with

experimental results for intermediate spin complexes rather than their high spin counterparts.

The calculated split in the para- hydrogens for the sextet imido complexes can be explained on the basis of coordination geometry and local symmetry differences between quartet and sextet complexes. These differences place the para-hydrogens in a more chemically and presumably magnetically different environment for the high spin complexes as compared to their intermediate spin counterparts. Figure 5.7 shows the geometry of quartet and sextet L^{Me}FeNAd, respectively.

Figure 5.7. Quartet (left) and sextet (right) L^{Me}FeNAd. Hydrogens (except para-hydrogens, which are pink in color) have been omitted for clarity.

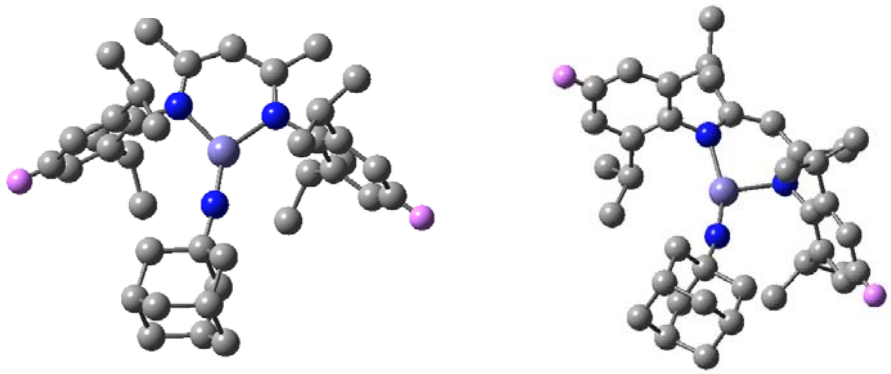

In the case of quartet L^{Me}FeNAd, Figure 5.7 (left), the molecule has local ~ C_{2v} symmetry about the iron center and both para hydrogens are at near equal distances from the paramagnetic Fe^{III} (Fe-H_1 = 6.12 Å and Fe-H_2 = 6.07 Å). As the dominant paramagnetic contribution (δ_{hf}) is very sensitive to distance from the proton to the paramagnetic center, we expect a single peak for the para hydrogens that integrates to two protons. In the case of the sextet complexes, Figure 5.7 (bottom), there is a much

greater distortion in the local symmetry about the iron and one para hydrogen is thus further from the metal center than the other chemically equivalent proton (Fe-H_1 = 6.38 Å and Fe-H_2 = 6.25 Å), thereby placing these in magnetically distinct environments, which will result in two different chemical shifts.

Taken together, these observations support the assignment of the dominant species in solution as a quartet. The calculated differences in ^{1}H NMR chemical shifts for the para hydrogens between L^{Me}FeNAd and L^{Me}Fe(4-t-Bu-Py)NAd are not large enough to make an unambiguous assignment in regards to coordination number. However no NMR peaks assignable to the 4-tert-butyl-pyridine are observed, implying a predominance of three-coordinate over four-coordinate imido complex in solution at the concentrations of 4-tert-butyl-pyridine that were investigated.

5.5 Mossbauer calculations

To support the experimental measurements of the Mossbauer spectra of the putative Fe^{III}-imido intermediates,[78] B3LYP[23,25] calculations with Wachters' all-electron basis (62111111/3311111/3111) for Fe, 6-311G* for carbon and nitrogen, and 6-31G* for hydrogen atoms[87] are carried out to calculate Mossbauer isomer shifts (δ_{Fe}). To calculate δ_{Fe}, it is necessary calculate the charge density at the iron nucleus, $\rho(0)$. The isomer shifts are then calculated via equation 5.2 derived for B3LYP calculations by Oldfield *et al.*[91]

$$\delta_{Fe} = -0.404\,[\rho(0) - 11614.16] \qquad (5.2)$$

The following table shows the calculated charge densities, $\rho(0)$ and isomer shifts δ_{Fe} for both three- and four-coordinate Fe-imide complexes at quartet and sextet spin states.

Table 5.5. Calculated Isomer Shifts for L^{Me}FeNAd and L^{Me}Fe(4-t-Bu-Py)NAd.

Nucleus#	$\rho(0)$	δ_{Fe} mm/s
L^{Me}FeNAd -IS	11613.13	0.40
L^{Me}FeNAd -HS	11613.16	0.42
L^{Me}Fe(4-t-Bu-Py)NAd -IS	11612.63	0.62
L^{Me}Fe(4-t-Bu-Py)NAd -HS	11612.72	0.58

IS = intermediate spin (quartet); HS = high spin (sextet);

A comparison of calculated and experimental isomer shifts has been done. An experimental shift of 0.47(4) mm/s, accounted for 75% of the total iron at equilibrium of the three and four coordinate Fe-imido complexes in solvent phase,[78] is in close agreement with the isomer shifts calculated for three-coordinate Fe-imido complexes. Similarly, there is a second observed experimental isomer shift of 0.63(8) mm/s, which accounted for 20% of the total iron. This latter value is in close agreement with the calculated isomer shifts for four-coordinate Fe-imido complexes. Thus, the calculated Mossbauer isomer shifts provide further support for the contention that three-coordinate Fe-imido complexes are the dominant equilibrium species in solution for low 4-tert-butyl-pyridine concentrations.

5.6 Results and Conclusions

A major motivation of this research is to determine the effects of multiplicity and coordination number of Fe^{III} on the reaction coordinate for C-H bond activation by Fe^{III}(β-diketiminate)-imido complexes. Experimental research by Holland *et al.*[78] has been interpreted to conclude that the four-coordinate Fe-imido is more active for C-H

bond scission versus a three-coordinate congener. A series of calculations are carried out on both computational models (DFT) as well full experimental complexes (hybrid DFT/molecular mechanics methods) to investigate the experimental proposals since it was not possible to isolate and structurally characterize any Fe^{III}-imido intermediates.

Calculations on full experimental models indicate that the ground state of $L^{Me}Fe(4^{t}BuPy)_x(=NAd)$ is as a quartet (intermediate) spin state for x = 0 and a sextet (high spin state) for x = 1. For the latter, four-coordinate imido complex the quartet and sextet states are very close in energy, with the latter only 2 kcal/mol higher in energy. Hence, we propose that C-H activation would be limited to the quartet surface for a three-coordinate imido complex as the sextet is 9 kcal/mol higher in energy. Furthermore, the ligation of a Lewis base such as 4-*tert*-butyl-pyridine makes the high spin (sextet) and the intermediate spin (quartet) states more energetically competitive, and thus the C-H activation event may potentially access both spin states when the Fe^{III} is four-coordinate. This is reminiscent of Shaik's two-state reactivity model for ferryl (FeO) species.[79]

The QM/MM calculations indicate that the change in spin state structure is due to a pyramidalization of the $L^{Me}Fe=NAd$ core upon coordination of the fourth ligand. This change in spin state results in greater spin density on the imido nitrogen for the high spin four-coordinate imido complex than the intermediate spin three-coordinate complex. Geometrical measurements for the four-coordinate sextet imido complex showed a longer Fe=N bond and more bent Fe=N-R moiety than the three-coordinate

quartet complex. These observations imply greater reactivity for the HS four-coordinate imido complex in C-H radical abstraction pathways.

Calculation of the N-H bond energies for the full models indicates a system that will activate only the weakest C-H bonds, consistent with experimental selectivity pattern. Furthermore, the steric constraints placed on the linear three-center N_{imido}•••H•••C active site of the calculated transition states permit access to only relatively nonhindered C-H bonds. Comparison of molecular mechanics calculations for activation of the *bis*-allylic C-H bonds of 1,4-cyclohexadiene, indene and 9,10-dihydroanthracene suggest that the latter substrate would be hindered in a transition state that contains a four-coordinate iron, but be less hindered for an imido active species with a three-coordinate iron.

Although ^{1}H NMR calculations showed moderate correlation with experimental observations, the use of approximations and constraints implies that the validity of the calculated chemical shifts must be viewed with caution. The calculated ^{1}H NMR chemical shifts using Oldfield's "locally dense" scheme are more consistent with a quartet ground state for the imido complex L^{Me}Fe=NAd, which is proposed to be the dominant species in solution at low concentrations of the fourth ligand.

Calculation of Mossbauer isomer shifts were more satisfactory than the ^{1}H NMR chemical shifts, and showed good correlation with experimental observations and gave strong support to the proposal of quartet, three- coordinate L^{Me}Fe=NAd being the dominant species at equilibrium.

Taken together, the present calculations support C-H activation by a four-coordinate iron-imido complex, yielding the counterintutitive and thus interesting conclusion that increased coordination number of the metal enhances the reactivity of the resultant complex. Furthermore, on the basis of the electronic structure parameters and calculated reaction coordinates, we propose that ligation of the fourth ligand enhances the activity of the system by making the "more reactive" high spin state of these formally Fe^{III} complexes more energetically accessible.

CHAPTER 6

CONCLUSIONS AND PROSPECTUS

The crux of this research is two fold: The first step is to determine the validity of computational techniques and apply the appropriate techniques to investigate the geometrical, thermodynamical and chemical properties of target species. The second step of my research deals with the application of the computational techniques to investigate and propose a good catalytic system for C-H bond activation and functionalization.

Methane being the least reactive and the major component of natural gas, its activation and conversion to functionalized products is of great scientific and economic interest in pure and applied chemistry. Thus C-H activation followed by C-C/C-X functionalization became crux of organic synthesis and transition metal catalysis.

From the observed results and conclusions of Chapter 3, DFT (density functional theory) methods are well suited to determine the thermodynamic as well as kinetic factors of a reaction. The obtained results are in good agreement with proposed mechanisms and chemical theory beyond. More over, the obtained results assist industrial catalysis and experimental chemistry with additional information: since C-X (X = halogens) bond cleavage is important in many metal catalyzed organic syntheses, the results obtained in this research helps in determining the selectivity (kinetic or thermodynamic) advantage. For example results obtained from Chapter 3 indicate that the thermodynamic advantage for C-F bond activation is significant over C-Cl bond cleavage. Similarly when C-P bond activation is considered, our results indicated that

C-X activation barrier is lower than C-H activation barrier. These results are interesting given the potential degradation pathways in industrially important phosphine ligands. These results initiated further studies of this type of research using a wide range of transition metal complexes. Transition metal initiated C-H and C-X bond activation of an alkyl derivative has been investigated at both theoretical[41b] and experimental levels of chemistry. The results obtained for calculations[41b] done using second row Zirconium metal systems are similar to the results discussed in Chapter 3 with Iridium metal systems. The obtained linearity gives the flexibility to use different metal systems over wide range of industrial and experimental bond activations as discussed above.

The results obtained from Chapter 4 gave a good support to the experimental results and verified the experimentally demonstrated[11,12,13] Ni-atom transfer mechanism from Ni=E (E = CH_2, NH, PH) activating complex to ethylene to form three-membered ring products. Since synthesis of azirdine, cyclopropane and phosphirane is vital in synthetic chemistry, the proposed reaction mechanism and the obtained results validate the application of late transition metal complexes in respective process.

The obtained results from DFT calculations increased the research scope of Ni=E activating complexes. These activating complexes can be used for the investigation of more useful commercial reactions like C-H bond activation. The kinetic and thermodynamic facts of the C-H bond activation of different commercially viable substrates like methane, cyclohexadiene etc., can be studied by parent Ni=E activating complexes. Furthermore, the possible increase in the efficiency of the catalyst can be investigated by tuning the Ni=E bond energy. Changing the substituents on the parent

ligand system and by increasing the coordination around metal center can attain this tuning. Various substituents with electron acceptor and electron donor nature should be used for further investigation.

The results obtained from Chapter 5 supported the argument that increase in metal coordination and electronic spin state increases catalytic activity of Fe^{III}-Imido complexes. These results not only supported the fact that DFT and multi-layer ONIOM methods are good to determine geometry and thermodynamics of meta-stable chemical complexes, but also gave a great support to spectroscopic calculations like NMR and Mossbauer calculations. Since in the present research the reactivity of LFe(III)-imido over C-H bond activation of cyclohexadiene substrate is studied, the possible extension of this research is to study the activity of LFe(III)-imido over stronger C-H bonds. Development of a better LFe(III)-imido system with weaker Fe-N bond will enhance the catalytic activity of LFe(III)-imido over stronger C-H bond activation. Factors like steric bulk around the metal center, decrease in electronic unsaturation and the size of the substrate plays a vital role in this research. Besides, development of these systems will allow to explore the reactions carried out by isovalant Fe=O systems in biological systems.

Thus application of DFT methods helped in determining the activity and properties of the present existing metal systems (Chapter 4). The performed calculations not only fabricated catalytic systems and directed experimental chemists (Chapter 3) for further experiments but also supported and scrutinized the experimental results (Chapter 5).

REFERENCES

1. Crabtree, R. H. *Chem. Reu.* 1985, *85*, 245.

2. Howell, J. A. S.; Burkinshaw, P. M. *Chem. Rev.* 1983, *83*, 557.

3. (a) Groves, J. T.; Takahashi, T. *J. Am. Chem. Soc.* 1983, *105*, 2073.

   (b) LaPointe, R. E.; Wolczanski, P. T.; Mitchell, J. F. *J. Am. Chem. Soc.* 1986, *108*, 6382. (c) Cummins, C. C. *Chem. Commun.* 1998, *1777*.

4. *Transition Metal Organomerallics in Organic Synthesis*; Alper, H., Ed.; Academic Press: New York, 1976.

5. Vaska, L.; DiLuzio, J. W. *J. Am. Chem. Soc.* 1962, *84*, 679.

6. Collman, J. P.; Hegedus, L. S.; Norton, J. R.; Finke, R. G. *Principles and Applications of Organotransition Metal Chemistry*. University Science Books; Mill Valley, CA, 1987. (b) Baranano, D.; Hartwig, J. F. *J. Am. Chem. Soc*. 1995, *117*, 2937. (c) Koo, K.; Hillhouse, G. L.; Rheingold, A. L. *Organometallics*, 1995, *14*, 456.

7. (a) Tanner, D, D.; Van Bostelen, P. B. *J. Org. Chem.* 1967, *32*, *1517*. (b) Taha, I. A. I.; Kuntz, R. R. *J. Phy. Chem,* 1969, *73*, 4406.

8. Cundari, T. R., Vaddadi, S. *Inorg. Chim. Acta.* 2004, *2863*, 357.

9. Kelm, D. H.; Walper, M. *Zeitschrift fuer Anorganische und Allgemeine Chemie* 1981, 483, 225.

10. (a) Wigley, D. E. *Prog. Inorg. Chem.* 1994, *42*, 239.

(b) MacBeth, C. A.; Golombek, A. P.; Young, V. G., Jr.; Yang, C.; Kuczera, K.; Hendrich, M. P.; Borovik, A. S. *Science* 2000, *289*, 938.

11. (a) Waterman, R.; Hillhouse, G. L. *Organometallics.* 2003, *23*, 5182.

(b) Waterman, R.; Hillhouse, G. L. *J. Am. Chem. Soc*. 2003, *125*, 13350.

12. Mindiola, D. J.; Hillhouse, G. L. *J. Am. Chem. Soc*. 2002, *124*, 9976.
13. Mindiola, D. J.; Hillhouse, G. L. *J. Am. Chem. Soc*. 2001, *123*, 4623.
14. In computational model, hydrogens have replaced the bulky t-butyl substituents on cyclic phosphino ethane ligand. This results (dhpe)Ni=E as computational model. (dhpe = dihydro phosphino ethane).
15. *Molecular modeling - Principles and Applications*, Leach. A.R., Longman, Harlow, UK, 1996.
16. (a) Thiel, W.; Voityuk, A. *Theor. Chim. Acta.*, 1992, *81*, 391.

    (b) Thiel, W.; Voityuk, A. *Int. J. Quantum Chem.*, 1992, 44, 807.
17. Stewart, J. J. P. *J. Comp. Chem.*, 1989, *10*, 209.
18. Hehre, W. J.; Yu, J. *Book of Abstracts,* 2002, 224th ACA National Meeting, Boston, MA, August 18-22.
19. (a) Kohn, W., Becke, A. D., Oarr, R. G. *J. Phys. Chem.* 1996, 100, 12974. (b) Parr, R. G.; Yang, W. *density functional theory of Atoms and Molecules;* Oxford: New York, 1989.
20. Hohenber, P.; Kohn, W. *Phys. Rev. B,* 1964, *136*, 864.
21. Kohn, W.; Sham, L. *J. Phys. Rev. A,* 1965, *140*, A1133.
22. Becke, A.D. *J. Chem. Phys.* 1992, *97*, 9173.
23. Quantum Theory of Molecular and Solids. Vol. 4: The Self-consistent Field for Molecular and Solids, Slater, J. C., McGraw-Hill, NY, 1974.
24. Becke, A. D. *Phys. Rev. A*, 1988, *38*, 3098.

25. Vosko, S. H.; Wilk, L.; Nussair, M. *Can. J. Phys.,* 1980, *58*, 1200.

26. Lee, C.; Yang. W.; Parr, R. G. *Phys. Rev. B,* 1981, *23*, 5048.

27. Svensson, M.; Humbel, S.; Froese, R. D. J.; Matsubara, T.; Sieber, S.; Morokuma, K. *J. Phys. Chem*. 1996, *100*, 19357.

28. (a) Kahn, L. R.; Baybutt, P.; Truhlar, D. G. *J. Chem. Phys.* 1976, *65*, 3826. (b) Krauss, M.; Stevens, W. *J. Annu. Rev. Phys. Chem.* 1984, *35*, 357.

29. (a) Stevens, W.; Basch, H.; Krauss, M. *J. Chem. Phys.,* 1984, *81*, 6026. (b) Stevens, W.; Basch, H.; Krauss, M.; Jasien, P. G. *Can. J. Chem*., 1992, 7*0*, 612. (c) Cundari, T. R.; Stevens, W. J. *J. Chem. Phys*., 1993, *98*, 5555.

30. (a) Frisch, M. J.; Trucks, G. W.; Schlegel, H. B.; Scuseria, G. E.; Robb, M. A.; Cheeseman, J. R.; Zakrzewski, V. G.; Montgomery, Jr., J. A.; Stratmann, R. E.; Burant, J. C.; Dapprich, S.; Millam, J. M.; Daniels, A. D.; Kudin, K. N.; Strain, M.C.; Farkas, O.; Tomasi, J.; Barone, V.; Cossi, M.; Cammi, R.; Mennucci, B.; Pomelli, C.; Adamo, C.; Cliord, S.; Ochterski, J.; Petersson, G. A.; Ayala, P. Y.; Cui, Q.; Morokuma, K.; Malick, D. K.; Rabuck, A. D.; Raghavachari, K.; Foresman, J. B.; Cioslowski, J.; Ortiz, J. V.; Stefanov, B. B.; Liu, G.; Liashenko, A.; Piskorz, P.; Komaromi, I.; Gomperts, R.; Martin, R. L.; Fox, D. J.; Keith, T.; Al-Laham, M. A.; Peng, C.Y.; Nanayakkara, A.; Gonzalez, C.; Challacombe, M.; Gill, P. M. W.; Johnson, B.; Chen, W.; Wong, M.W.; Andres, J. L.; Gonzalez, C.; Head-Gordon M.; Replogle, E. S.; Pople, J. A.; *Gaussian Inc.,* Pittsburgh, PA, 1998. (b) Frisch, M. J.; Trucks, G. W.; Schlegel, H. B.; Scuseria, G. E.; Robb, M. A.; Cheeseman, J. R.;

Montgomery, Jr., J. A.; Vreven, T.; Kudin, K. N.; Burant, J. C.; Millam, J. M.; Iyengar, S. S.; Tomasi, J.; Barone, V.; Mennucci, B.; Cossi, M.; Scalmani, G.; Rega, N.; Petersson, G. A.; Nakatsuji, H.; Hada, M.; Ehara, M.; Toyota, K.; Fukuda, R.; Hasegawa, J.; Ishida, M.; Nakajima, T.; Honda, Y.; Kitao, O.; Nakai, H.; Klene, M.; Li, X.; Knox, J. E.; Hratchian, H. P.; Cross, J. B.; Bakken, V.; Adamo, C.; Jaramillo, J.; Gomperts, R.; Stratmann, R. E.; Yazyev, O.; Austin, A. J.; Cammi, R.; Pomelli, C.; Ochterski, J. W.; Ayala, P. Y.; Morokuma, K.; Voth, G. A.; Salvador, P.; Dannenberg, J. J.; Zakrzewski, V. G.; Dapprich, S.; Daniels, A. D.; Strain, M. C.; Farkas, O.; Malick, D. K.; Rabuck, A. D.; Raghavachari, K.; Foresman, J. B.; Ortiz, J. V.; Cui, Q.; Baboul, A. G.; Clifford, S.; Cioslowski, J.; Stefanov, B. B.; Liu, G.; Liashenko, A.; Piskorz, P.; Komaromi, I.; Martin, R. L.; Fox, D. J.; Keith, T.; Al-Laham, M. A.; Peng, C. Y.; Nanayakkara, A.; Challacombe, M.; Gill, P. M. W.; Johnson, B.; Chen, W.; Wong, M. W.; Gonzalez, C.; and Pople, J. A.; Gaussian, Inc., Wallingford CT, 2004.

31. (a) Koga, N.; Morokuma, K. *J. Am. Chem. Soc.* 1993, *115*, 6883. (b) Koga, N.; Morokuma, K. *Chem. Rev.* 1991, *91*, 823. (c) Torrent, M.; Sola, M.; Frenking, G. Chem. Rev. 2000, *100*, 823.

32. (a) Janowicz, A. H.; Bergman, R. G. *J. Am. Chem. Soc.* 1983,*105*, 3929.
(b) Janowicz, A. H.; Bergman, R. G. *J. Am. Chem. Soc.* 1982, *104*, 352.
(c) Jones, W. D.; Feher, F. J. *Organometallics* 1983, *2*, 562.
(d) Hoyano, J. K.; Graham, W. A. G.. *J. Am. Chem. Soc.* 1982, *104*, 3723.

33. Oxidative addition/reductive elimination of C-halogen, C-O and C-N bonds is relevant to catalytic amination and etheration of aryl halides as in the Hartwig-

Buchwald synthesis. Carbon-halogen oxidative addition also occurs in the catalytic cycle of other organic transformations beginning from aryl halides, for example, the Suzuki reaction.

(a) Miyaura, N.; Suzuki, A. *Chem. Rev.* 1995, *95*, 2457.

(b) Suzuki, A. *J. Organomet. Chem.* 1999, *576*, 147.

(c) Yang, B. H.; Buchwald, S. L. *J. Organomet. Chem.* 1999, *576*, 125.

(d) Wolfe, J. P.; Wagaw, S.; Marcoux, J.-F.; Buchwald, S. L. *Acc. Chem. Res.* 1998, *31*, 805.

(e) Hartwig, J. F. *Acc. Chem. Res.* 1998, *31*, 852.

(f) Hartwig, J. F. *Pure Appl. Chem.* 1999, *71*, 1417.

34. (a) Su, M-D.; Chu, S-Y. *J. Am. Chem. Soc.* 1997, *119*, 10178.

(b) Crespo, M.; Martinez, M.; Sales, J. *Organometallics* 1993, *12*, 4297.

(c) Richmond, T. G.; Osterberg, C. E.; Arif, A. M. *J. Am. Chem. Soc.* 1987, *109*, 8091.

(d) Grushin, V. V.; Alper, H. *Topics Organomet. Chem.* 1999, *3*, 193.

(e) Dorta, R.; Shimon, L. J. W.; Rozenberg, H.; Milstein, D. *Euro. J. Inorg. Chem.* 2002, *7*, 1827.

35. Ugo, R.; Pasini, A.; Fusi, A.; Cenini, S. *J. Am. Chem. Soc.* 1972*, 94*, 7364.

36. Representative examples of carbon-sulfur oxidative addition:

(a) Dobrzynski, E. D.; Angelici, R. J. *J. Organomet. Chem.* 1974, *76*, C53.

(b) Osakada, K.; Maeda, M.; Nakamura, Y.; Yamamoto, T.; Yamamoto, A. *J. Chem. Soc., Chem. Comm.* 1986, 442.

(c) Gosselink, J. W.; Bulthuis, H.; Van Koten, G. *J. Chem. Soc., Dalton,* 1981, 1342.

(d) Gosselink, J. W.; Van Koten, G.; Brouwers, A. M. F.; Overbeek, Ok. *J. Chem. Soc., Dalton* 1981, 342.

37. Hori, T. *Seikagaku.* 1971*, 43*, 1009.

38. (a) Herrmann, W. A.; Brossmer, C.; Oefele, K.; Beller, M.; Fischer, H. J. *Organomet. Chem.* 1995, *491*, C1.

(b) Garrou, Philip E. *Chem. Rev.* 1985, *85*, 171.

(c) Dubois, R. A.; Garrou, P. E.; Lavin, K. D.; Allcock, H. R. *Organometallics* 1986, *5*, 460.

39. Yamamoto, A. *Organotransition Metal Chemistry*, Wiley: New York, 1985, *240*.

40. Chen, J-Y.; Halpern, J. *J. Am. Chem. Soc. 1971*, *93*, 4939.

41. (a) Brookhart, M.; Green, M. L. H.; Wong, L. L. *Prog. Inorg. Chem.* 1988, *36*, 1. (b) Crabtree, R. H.; Holt, E. M.; Lavin, M.; Morehouse, S. M. *Inorg. Chem.* 1985, *24*, 1986.

42. Recent examples employing the Steven ECP methodology include the following.

(a) Vela. J; Vaddadi, S.; Kingsley, S.; Flaschenriem, C. J.; Lachicotte, R. J.; Cundari, T. R.; Holland, P. L. *Angew. Chem. Int. Ed.* 2006, *45*, 1607.

(b) Cundari, T. R.; Pierpont, A. W. *Intern. Journ. Quant. Chem.* 2006, *106*, 1611.

43. Riehl, J. F.; Jean, Y.; Eisenstein, O.; Pelissier, M. *Organometallics* 1992, *11*, 729.

44. Allen, F. H.; Davies, J. E.; Galloy, J. J.; Johnson, O.; Kennard, O.; Macrae, C. F.; Mitchell, E. M.; Mitchell, G. F.; Smith, J. M.; Watson, D. G. *J. Chem. Info. Comp. Sci.* 1991, *31*, 187.

45. Cundari, T. R. *J. Am. Chem. Soc.* 1994, *116*, 340.

46. Zaric, S.; Hall, M. B. *J. Phys. Chem. A* 1997, *101*, 4646.

47. Reed, A. E.; Weinhold, F. *J. Chem. Phys.* 1985, *83,* 1736.

48. Theoretical Study of Group Transfer from Multiply Bonded Nickel Complexes to Ethylene. Sridhar Vaddadi and Thomas R. Cundari. – *in Press* THEOCHEM.

49. (a) Wolfe, J. P.; Wagaw, S.; Marconx, J-F.; Buchwald, S. L. *Acc. Chem. Res.* 1998, 31, 805. (b) Hartwig, J. F. *Acc. Chem. Res.* 1998, *31*, 852.

50. (a) Groves, J. T.; Takahashi, T. *J. Am. Chem. Soc.* 1983, *105*, 2073. (b) LaPointe, R. E.; Wolczanski, P. T.; Mitchell, J. F. *J. Am. Chem. Soc.* 1986, *108*, 6382. (c) Cummins, C. C. *Chem. Commun.* 1998, *17*, 1777. (d) DuBois, J.; Tomooka, C. S.; Hong, J.; Carreira, E. M. *Acc. Chem. Res.* 1997, *30*, 364.

51. Holm, R. H. *Chem. Rev.* 1987, *87*, 1401.

52. (a) Wigley, D. E. *Prog. Inorg. Chem.* 1994, *42*, 239. (b) MacBeth, C. A.; Golombek, A. P.; Young, V. G., Jr.; Yang, C.; Kuczera, K.; Hendrich, M. P.; Borovik, A. S. *Science* 2000, *289*, 938.

53. Jenkins, D. M.; Betley, T. A.; Peters J. C. *J.Am.Chem.Soc.* 2002, *124*, 11238.

54. Mayer, J. M. *Comm. Inorg. Chem.* 1988, *8*, 125.

55. (a) Evans, D. A.; Faul, M. M.; Bilodeau, M. T. *J. Org. Chem.* 1991, *56*, 6744.

(b) Evans, D. A.; Faul, M. M.; Bilodeau, M. T.; Anderson, B. A.; Barnes, D. M. *J. Am. Chem. Soc*. 1993, *115*, 5328. (c) Evans, D. A.; Faul, M. M.; Bilodeau, M. T. *J. Am. Chem. Soc*. 1994, *116*, 2742.

56. Li, Z.; Consuer, K. R.; Jacobsen, E. J. *J. Am. Chem. Soc*. 1993, *115*, 5326.

57. Brandt, P.; Soedergre, J. M.; Andersson, G. P.; Norrby, P-O. *J. Am. Chem. Soc.* 2000, 112, 8013.

58. Simmons, H.E.; Smith, R.D. *J. Am. Chem. Soc*. 1959, *81*, 4265

59. (a) Mathey, F. *Chem. Rev*. 1990, *90*, 997. (b) Golobov, Y. G.; Gusar, N. I.; Tarasevich, A. S. *Russ. Chem. Rev*. 1983, *52*, 787.

60. Wagner, R. I.; Freeman, L. V. D.; Goldwhite, H.; Rowsell, D. G. *J. Am. Chem. Soc.* 1967, *89*, 1102.

61. Chan, S.; Goldwhite, H.; Keyzer, H.; Rowsell, D. G.; Tang, R. *Tetrahedron* 1969, *91*, 17.

62. (a) Marinette, A.; Charrier, C.; Mathey, F.; Fischer, J. *Organometallics* 1985, *4*, 2134. (b) Marinette, A.; Mathey, F. *Organometallics* 1984, *3*, 456.

63. (a) Carmichael, D.; Hitchcock, P. B.; Nixon, J. F.; Mathey, F.; Ricard, L. *J. Chem. Soc.*, *Dalton Trans.* 1993, *12*, 1811. (b) Ajulu, F. A.; Carmichael, D.; Hitchcock, P. B.; Mathey, F.; Meidine, M. F.; Nixon, J. F.; Ricard, L.; Riley, M. L. *J. Chem. Soc., Chem. Commun.* 1992, 750. (c) Al Juaid, S. S.; Carmichael, D.; Hitchcock, P. B.; Marinetti, A.; Mathey, F.; Nixon, J. F. *J. Chem. Soc., Dalton Trans.* 1991, 905.

64. Ehlers, A. W.; Goumans, T. P. M.; Lammertsma, K. *J. Organomet. Chem.* 2005, *690*, 5517.

65. (a) Brunkan, N. M.; Brestensky, D. M.; Jones, W. D. *J. Am. Chem. Soc.* 2004, *126*, 3627. (b) Brauer, D. J.; Kruger, C. *J. Organomet. Chem.* 1974, *77*, 423.

66. Lin, B. L.; Clough, C. R.; Hillhouse, G. L. *J. Am. Chem. Soc.* 2002, *124*, 2890.

67. Repeated attempts to find a [1+2] addition transition state were unsuccessful, and resulted in minima and transition states that duplicate those already found.

68. Some other recent examples of three-coordinate complexes include:

(a) Sydora, O. L.; Wolczanski, P. T.; Lobkovsky, E. B.; Buda, C.; Cundari, T. R. *Inorg. Chem.* 2005, *44*, 2606 (b) Mindiola, D. J.; Hillhouse, G. *J. Am. Chem. Soc.* 2002, *124*, 9976.

69. (a) Vela, J.; Vaddadi, S.; Cundari, T. R.; Smith, J. M.; Gregory, E. A.; Lachicotte, R. J.; Flaschenriem, C. J.; Holland, P. L. *Organometallics* 2004, *23,* 5226 (b) Smith, J. M.; Lachicotte, R. J.; Pittard, K. A.; Cundari, T. R.; Lukat-Rodgers, G.; Rodgers, K. R.; Holland, P. L. *J. Am. Chem. Soc.* 2001, *123*, 9222.

70. Bourget-Merle, L.; Lappert, M. F.; Severn, J. R. *Chem. Rev.* 2002, *102,* 3031.

71. (a) Bryndza, H. E.; Tam, W. *Chem. Rev.* 1988, *88*, 1163 (b) Borovik, A. S.; Powell, D. R.; Lucas, R. L. *J. Am. Chem. Soc*. 2005, *127*, 11596.

72. (a) Hartwig, J. F. *Acc .Chem. Res.* 1998, *31*, 852-860; (b) Hartwig, J. F. *Angew. Chem., Int. Ed.* 1998, *37*, 2046-2067.

73. Conner, D.; Jayaprakash, K. N.; Cundari, T. R. ; Gunneo, T. B. *Organometallics* 2004, *43, 3306.*

72. Eckert, N. A.; Smith, J. M.; Lachicotte, R. J.; Holland, P. L. *Inorg. Chem.* 2004, *43*, 3306.

75. (a) Buckner, S. W.; Gord, J. R.; Freiser, B. S. *J. Am. Chem. Soc.* 1998, *110*, 6606. (b) Mayer, M. J. *Comments Inorg. Chem.* 1988, *8*, 125-135. (c) Hu and Meyer attribute the paucity of examples to a mismatch between the hard imido ligand and soft late transition metal centers. Hu, X.; Meyer, K. *J. Am. Chem. Soc.* 2004, *126*, 16322.

76. (a) Verma, A. K.; Nazif, T. N.; Achim, C.; Lee, C. S. *J. Am. Chem. Soc.* 2000, *122,* 11013. (b) Brown, S. D.; Betley, T. D.; Peters, J. C.; *J. Am. Chem. Soc.* 2003, *125*, 322. (c) Brown, S. D.; Peters, J. C. *J. Am. Chem. Soc*. 2004, *126*, 4538. (d) Brown, S. D.; Peters, J. C. *J. Am. Chem. Soc*. 2005, *127*, 1913. (e) Brown, S. D.; Mehn, M. P.; Peters, J. C. *J .Am. Chem. Soc*. 2005, *127*, 13146. (f) Mindiola, D. J.; Hillhouse, G. *Chem. Comm.* 2002, *124*, 1840. (g) Buckner, S. W.; Freiser, B. S. *J. Am. Chem. Soc.* 1987, *109*, 4715. (h) Schwarz, H.; Schroder, D.; Kretzschmar, I.; Bronstrup, M. *Helvet. Chim. Acta.* 1988, *81*, 2348. (i) Kogut, E.; Wiencko, H. L.; Zhang, L.; Cordeau, D.; Warren, T. H. *J. Am. Chem. Soc.* 2005, *127*, 11248. (j) Thyagarajan, S.; Shay, D. T.; Incarvito, C. D.; Rheingold, A. L.; Theopold, K. H. *J. Am. Chem. Soc,* 2003, *125,* 4440. (k) Jensen, M. P.; Mehn, M. P.; Que, L. *Angew. Chem. Int. Ed.* 2003, *42*, 4357. (l) Betley, T. A.; Peters, J. C. *J. Am. Chem. Soc.* 2003, *125*, 10782.

77. Brown, S. D.; Peters, J. C. Chemistry of tris(phosphino)borate supported iron compounds featuring metal-nitrogen multiple bonding. A*bstracts of Papers*, 227th ACS National Meeting, Anaheim, CA, 2004.

78. Eckert, N. A.; Vaddadi, S.; Stoian, S.; Flaschenriem, C. J.; Munck, E.; Cundari, T. R.; Holland, P. L. Hydrogen Atom Abstraction by an Fe(III) Imido Intermediate. GEN-288. 32nd Northeast Regional Meeting of the American Chemical Society, Rochester, NY, 2004.

79. (a) Shaik. S.; Filatov. M. *Chem. Eur. J.* 1998, *4*, No.2, 193. (b) Sono, M.; Roach, M. P.; Coulter, E. D.; Dawson, J. H. *Chem Rev.* 1996, *96*, 2841.

80. Yoshizawa, K. *Coord. Chem. Rev.* 2002, *226*, 251.

81. Filatov, M.; Shaik, S.; *J. Phys. Chem. A*, 1998, *102,* 3835.

82. Casewit, C. J.; Colwell, K. S.; Rappé, A. K. *J. Am. Chem. Soc.* 1992, *114*, 10035. (b) Rappé, A. K.; Casewit, C. J.; Colwell, K. S.; Goddard, W. A., III; Skiff, W. M. *J. Am. Chem. Soc.* 1992, *114*, 10024.

83. Panda, A; Stender, M; Wright, R. J.; Olmstead, M. M.; Klavins, P; Power, P. P. *Inorg. Chem.* 2002, *41*, 3909.

84. Schrodinger, Inc., Portland, OR, JAGUAR v3.5, 1998.

85. HyperChem(TM) Professional 7.51, Hypercube, Inc., 1115 NW 4th Street, Gainesville, Florida 32601, USA

86. Curtiss, L. A.; Raghavachari, K; Redfern, P. C.; Rassolov, V.; Pople, J. A.; *J. Chem. Phys.* 1998, *109*, 7764.

87. Mao, I.; Zhang, Y.; Oldfield, E. *J. Am. chem. Soc.* 2002, *124*, 13911.

88. Wolinski, K.; Hinton, J. F.; Pulay, P. *J. Am. Chem. Soc.* 1990, *112,* 8251.

89. (a)Godbout, N.; Havlin, R.; Salzmann, R.; Debrunner, P. G.; Oldfield, E. *J. Phys. Chem. A* 1998, *102*, 2342. (b)Havlin, R. H.; Godbout, N.; Salzmann, R.; Wojdelski,

M.; Arnold, W.; Schulz, C. E.; Oldfield, E. *J. Am. Chem. Soc.* 1998, *120*, 3144. (c) Godbout, N.; Sanders, L. K.; Salzmann, R.; Havlin, R. H.; Wojdelski, M.; Oldfield, E. *J. Am. Chem. Soc.* 1999, *121*, 3829.

90. (a)Wachters, A. J. H. *J. Chem. Phys.* 1970, *52*, 1033-1036. Wachters, A. J. H. IBM Technol. Report RJ584; 1969. (b) Basis sets were obtained from the Extensible Computational Chemistry Environment Basis Set Database, Version 1.0, as developed and distributed by the Molecular Science Computing Facility, Environmental and Molecular Sciences Laboratory which is part of the Pacific Northwest Laboratory, P.O. Box 999, Richland, WA 99352, USA and funded by the U.S. Department of Energy. The Pacific Northwest Laboratory is a multiprogram laboratory operated by Battelle Memorial Institute for the U.S. Department of Energy under contract DE-AC06-76RLO 1830. Contact David Feller or Karen Schuchardt for further information.

91. Mao, I.; Zhang, Y.; Oldfield, E. *J. Am. chem. Soc.* 2002, *124*, 7829.